

Nuclear versus integrated spectroscopy of galaxies in the *Herschel* Reference Survey.★ ★★

G. Gavazzi¹, G. Consolandi¹, S. Belladitta^{2,3}, A. Boselli⁴, and M. Fossati^{5,6}

¹ Università degli Studi di Milano-Bicocca, Piazza della Scienza 3, 20126 Milano, Italy
e-mail: giuseppe.gavazzi@mib.infn.it

² DiSAT, Università degli Studi dell'Insubria, Via Valleggio 11, 22100 Como, Italy

³ INAF - Osservatorio Astronomico di Brera, via Brera, 28, 20159 Milano, Italy
e-mail: silvia.belladitta@brera.inaf.it

⁴ Aix Marseille Université, CNRS, LAM (Laboratoire d'Astrophysique de Marseille) UMR 7326, F-13388, Marseille, France

⁵ Max-Planck-Institut für Extraterrestrische Physik, Giessenbachstrasse, D-85748 Garching, Germany

⁶ Universitäts-Sternwarte München, Schenierstrasse 1, D-81679 München, Germany

Received; accepted

ABSTRACT

Context. The determination of the relative frequency of active galactic nuclei (AGN) versus other spectral classes, for example, HII region-like (HII), transition objects (TRAN), passive (PAS), and retired (RET), in a complete set of galaxies in the local Universe is of primary importance to discriminate the source of ionization in the nuclear region of galaxies.

Aims. Here we aim to provide a spectroscopic characterization of the nuclei of galaxies belonging to the *Herschel* Reference Survey (HRS), a volume and magnitude limited sample representative of the local Universe, which has become a benchmark for local and high- z studies, for semianalytical models and cosmological simulations. The comparison between the nuclear spectral classification and the one determined on the global galactic scale provides information about how galaxy properties change from the nuclear to the outer regions. Moreover, the extrapolation of the global star formation (SF) properties from the SDSS fiber spectroscopy compared to the one computed by $H\alpha$ photometry can be useful for testing the method based on aperture correction for determining the global star formation rate (SFR) for local galaxies.

Methods. By collecting the existing nuclear spectroscopy available from the literature, complemented with new observations obtained using the Loiano 1.52m telescope, we analyze the 322 nuclear spectra of HRS galaxies.

Results. Using two diagnostic diagrams (the BPT and the WHAN) we provide a nuclear and an integrated spectral classification for the HRS galaxies. The BPT and the WHAN methods for nuclei consistently give a frequency of 53-64% HII, around 21-27% AGNs (including TRAN), and 15-20% of PAS (including RET), whereas for integrated spectra they give 69-84% HII, 4-11% of AGNs and 12-20% PAS.

Conclusions. We find that the fraction of AGNs increases with stellar mass, such that at $M_* \gtrsim 10^{10.0} M_\odot$ ~66% of the LTGs are AGNs or TRAN.

Key words. Galaxies: evolution – Galaxies: fundamental parameters – Galaxies: star formation

1. Introduction

Characterizing the nuclear properties of galaxies in the local Universe, that is, establishing the mass dependence of the relative frequency of active galactic nuclei (AGN) ionized by supermassive black holes with respect to HII region-like nuclei excited by young stars, or with respect to galaxies ionized by old stars, is an urgent task of today's research in astrophysics (see e.g., Kauffmann et al. 2003b, hereafter K03). There is a clear need to establish the frequency of AGNs of various types, in different environments, locally and from a cosmological perspective, to improve our understanding of galaxy assembly. As Boselli et al. (2010) pointed out, observing the local Universe is relevant because it represents the endpoint of galaxy evolution,

providing important boundary conditions to models and simulations. Galaxies can only be completely characterized at low-redshift or by multifrequency observations. Moreover, dwarf galaxies can only be observed locally. In recent years, considerable effort has been made to select representative samples of galaxies, like SINGS (Kennicutt et al. 2003), the recent KINGFISH (Kennicutt et al. 2011), and VNGS (Bendo et al. 2012), to study the properties of the local Universe. In recent years, the *Herschel* Reference Survey (HRS) (Boselli et al. 2010a) has become a benchmark for the representation of the properties of local galaxies (Hughes, T. M. et al. 2013, Boquien et al. 2014, Ciesla et al. 2016), and has therefore become a reference for comparing observations of local galaxies with those of increasing redshift (Bassett et al. 2017, Fossati et al. 2017, Schreiber et al. 2016) or resulting from simulations (Cattaneo et al. 2017, Fontanot et al. 2017, Lagos et al. 2016). The HRS has been observed with SPIRE (250, 350, 500 μm) (Ciesla et al. 2012, 2013) and with PACS (100, 160 μm) (Cortese et al. 2014) on board *Herschel*: At $D \leq 30$ Mpc the angular resolution of

* based on observations taken at the 1.5m Loiano telescope belonging to the Bologna Observatory.

** Table A4 is only available in electronic form at the CDS via anonymous ftp to cdsarc.u-strasbg.fr (130.79.128.5) or via http://cdsweb.u-strasbg.fr/cgi-bin/qcat?J/A+A/

SPIRE (4 arcmin) allows us to resolve the different galaxy components, such as nuclei, bulges, discs and spiral arms. The HRS is a volume-limited sample and is k -band selected, therefore, by design, it is suitable for statistical studies of the multifrequency properties of local galaxies. Many surveys have been done to cover the whole sample in different bands: FUV and NUV photometry obtained from GALEX is reported by Cortese et al. (2012); 24-160 μm photometry from MIPS is given by Bendo et al. (2012); Spitzer/IRAC photometry is reported by Ciesla et al. (2014); Boselli et al. (2014) report the gas properties (HI and CO) of the HRS, whereas Boselli et al. (2015, hereafter B15) describe an $H\alpha$ imaging survey of the full HRS. Finally Boselli et al. (2013) give the integrated (drift-mode) spectroscopy of the HRS. Conversely no systematic information is available from the literature on the nuclear spectroscopic classification of the HRS, a task that we tackle in this paper. Not all the 322 galaxies constituting the HRS have been observed spectroscopically so far (only 277/322 objects). In this paper we complete the HRS by presenting new nuclear long-slit spectroscopy for 45 galaxies, 25 of which in the whole optical range (from $H\beta$ to [SII]) and 20 only in the red band near $H\alpha$. Generally, the classification of galaxies based on their optical nuclear spectra is performed using the BPT (Baldwin, Phillips & Terlevich, 1981) diagnostic diagram, which requires the measurement of different spectral lines: $H\beta$, [OIII] λ 5007, $H\alpha$, [NII] λ 6583.4 and [SII] λ 6717,6731. In this diagram AGNs are distinguished from HII-region-like nuclei using the ratio [NII]/ $H\alpha$, while strong AGNs (sAGN) can be separated from the weaker (weak AGNs or wAGN) low-ionization nuclear emission-line region (LINERs, Heckman et al. 1980) using the ratio [OIII]/ $H\beta$. There is also a recent two-line diagnostic diagram, named WHAN, which is based only on the [NII]/ $H\alpha$ ratio combined with the equivalent width (EW) of the $H\alpha$ line. It was introduced by Cid Fernandes et al. (2010, 2011) to divide both strong and weak AGNs from *fake AGNs*, namely the retired galaxies (RET), whose ionization mechanism is probably provided by an old stellar population (Capetti & Baldi 2011). Using the BPT and the WHAN diagrams, we obtain a robust determination of the frequency of AGNs in a complete sample of local late-type galaxies (LTGs) and compare it with the frequency of HII-region-like nuclei as a function of stellar mass.

Moreover the comparison between the nuclear spectral classification and the one determined on the global galactic scale provides information about how galaxy properties change from the nuclear to the outer regions. The issue is hotly debated and only spectroscopy obtained with Integral Field Units (IFU) such as MaNGA (Belfiore et al. 2016, 2017; Sanchez et al. 2017), CALIFA (Sánchez et al. 2016) and SAMI (Richards et al. 2016) will bring the issue to an end. These surveys have confirmed previous claims that regions of low ionization conditions can in fact extend to the bulges of galaxies and even further, mimicking the presence of AGNs, being in fact due to old post-AGB stars.

We compare the global with the nuclear properties of HRS galaxies adopting a method similar to Moustakas et al. (2010) who used long-slit spectroscopy, while Iglesias-Páramo et al. (2013, 2016) adopted the two-dimensional (2D) spectroscopy. The availability of the global properties of HRS galaxies allows us to test the program of Brinchmann et al. (2004, hereafter B04) who claimed that a satisfactory estimate of the global star formation rate (SFR) of galaxies in the local Universe ($z < 0.2$) can be achieved using SDSS fiber spectroscopy, once corrected for aperture effects using SDSS photometry (e.g., *cmodel* - fiber colors), both quantities being available for hundreds of thousands of local galaxies thanks to the SDSS.

The paper is structured as follows: in section 2 we describe the sample, in section 3 we outline the data reduction, in section 4 we present the results, and in section 5 the discussion and conclusions. A description of the tables provided is given in the appendix. Standard cosmology is assumed, with $H_0 = 73$ km/s/Mpc.

The spectroscopic data presented in this work, as well as those collected at other frequencies, are available to the community through the HeDaM database (<http://hedam.lam.fr/HRS/>).

2. The sample

The sample of galaxies analyzed in this work is the *Herschel* Reference Survey (HRS) (Boselli et al. 2010a; the reader should refer to this paper to find the catalog names of HRS galaxies). It consists of a volume limited ($15 < Dist < 25$ Mpc) sample of 322 galaxies, located in the sky region in the ranges $10\text{h}17\text{m} \downarrow$ R.A.(2000) \downarrow $14\text{h}43\text{m}$ and $-6^\circ \downarrow$ dec \downarrow 60° (see Fig. 1), of which 64 are early-type galaxies (ETGs: E, S0 and S0a) and 258 are late-type galaxies (LTGs: Sa-Sd-Im-BCD).¹ All LTGs with a 2MASS K band total magnitude $K_{S\text{tot}} \leq 12$ mag have been selected and all ETGs with $K_{S\text{tot}} \leq 8.7$ mag have been included. The stellar mass range of HRS galaxies is: $5 \times 10^8 \leq M_* \leq 10^{11.3} M_\odot$. The sample spans a large range of environments: it includes the Virgo cluster, many galaxy groups, as well as isolated objects. In the Virgo cluster region ($12\text{h} \downarrow$ R.A. \downarrow 13h and $0^\circ \downarrow$ dec \downarrow 18°), the sample includes all galaxies with $vel \downarrow$ 3000 km/s and those belonging to cluster A, the North (N) and East (E) clouds, the southern extension (S; at 17 Mpc) and Virgo B (23 Mpc), where the subgroup membership has been taken from Gavazzi et al. (1999a). The W and M clouds, at a distance of 32 Mpc, have been excluded. In the sky projection map of Fig. 1, the Virgo cluster region, which includes 148 HRS objects from Virgo A, Virgo B, the N and E clouds and the S extension, is easily recognizable as the density enhancement at $RA \approx 190$ and $Dec \approx 10$.

2.1. Data from the literature

Most of HRS nuclear optical spectra were found in the literature. In particular, 163 spectra were downloaded in FITS format from the SDSS DR13 and DR12 database (Albaret et al. 2016); 114 spectra were found in the NASA/IPAC Extragalactic Database (NED) and 104 of these are taken from Ho et al. (1997). For these galaxies, the double spectrograph on the Hale 5m telescope at Palomar Observatory yielded simultaneous spectral coverage of $\sim 4230\text{-}5110\text{\AA}$ and $\sim 6210\text{-}6860\text{\AA}$, with a spectral resolution of $\sim 4\text{\AA}$ in the blue and $\sim 2.5\text{\AA}$ in the red. We joined the blue and red spectra by projecting them on a common wavelength solution and by performing a linear interpolation between the average flux of the last ten pixels of the blue spectrum and the first ten of the red spectrum. HRS-070, 072, 209, 265, 275, 288 and 284 have been observed with the 3.9m Anglo Australian Telescope (AAT) by Jones et al. (2009). HRS-193 was observed by Falco et al. 2000 with the Z-Machine at Mt. Hopkins 1.5m telescope (Arizona). HRS-251 was observed by Kim & Veilleux (1995) with the 2.2m telescope at the University of Hawaii. HRS-271 is part of the work of Jansen et al. (2000) who observed 196 nearby galaxies with the FAST instrument at Tillinghast 1.5m telescope

¹ With respect to the original sample given in Boselli et al. (2010a), we revised the morphological classification for some HRS galaxies: HRS-032, HRS-090, HRS-202, HRS-229 and HRS-291 become ETGs, while HRS-256 becomes LTG. After this revision, the LTGs are 254 and the ETGs are 68. In this work we use this new number for our analysis.

on Mt. Hopkins. Finally the remaining 45 spectra were observed by us with the 1.52m Cassini telescope at Loiano (Bologna) and their spectrum is published for the first time in this paper. Filled symbols in Fig. 1 represent these 45 HRS targets.

3. Long-slit nuclear spectroscopy: observations and data reduction

Nuclear spectroscopic observations of 45 HRS galaxies that were found neither in the SDSS spectroscopic catalog nor within the NED database, were obtained by us during several observing campaigns from 2000 to 2017 using the Bologna Faint Object Spectrograph and Camera (BFOSC, Gualandi & Merighi 2001) mounted on the 152cm F/8 Cassini Telescope located in Loiano, belonging to the Observatory of Bologna. Following the work of Gavazzi et al. 2011, 2013, these are long-slit spectra taken through a slit of 2 arcsec width and 12.6 arcmin length, combined with an intermediate-resolution red-channel grism (G8; $R \sim 2200$) covering the 6100 - 8200 Å portion of the spectrum containing the $H\alpha$, [NII], and [SII] lines. Twenty-five of these galaxies were also observed with the same instrument during six nights in April and May, 2017, (see Table A for details), using a blue-channel grism (G7) providing ($R \sim 1400$) cover from 4200 to 6600 Å. The observing log of these 45 galaxies is given in Table A.

BFOSC is equipped with a back illuminated EEV LN/1300-EB/1 CCD detector of 1300x1340 pixels, reaching 90% QE near 5500 Å and 70% QE near 4000 Å. For the spatial scale of 0.58 arcsec/pixel, and a dispersion of 8.8 nm/mm, the resulting spectra have a resolution of 1.6 Å/pix for G8 and a dispersion of 11 nm/mm, with a resolution of 1.9 Å/pix for G7.

Exposures of 2-7 minutes (G8) and 7-15 min (G7) were repeated typically three times to remove cosmic ray hits. The slit was generally set in the E-W direction and the typical seeing conditions at Loiano ranged from 1.5 to 2.5 arcsec. The wavelength calibration was secured by means of frequent exposures of a He-Ar hollow-cathode lamp and was further refined using bright OH sky lines. The spectrograph response (sensitivity function) was obtained by daily exposures of the stars Feige34 and Hz44 (Massey et al. 1988). The spectra were not flux calibrated, and measurements of the lines EW were derived, along with flux ratios of adjacent lines, namely [OIII]/H β , [NII]/H α and [SII]/H α .

The spectra were reduced using standard IRAF procedures. To derive the wavelength calibration we used the tasks *identify*, *reidentify*, and *fitcoord* on the hollow-cathode lamp exposures, and the 2D wavelength solution was transferred to the galaxy exposures by means of the task *transform*. After verification of the wavelength calibration on several known sky lines, the sky was subtracted using *background*. One-dimensional (1D) nuclear spectra were extracted from the 2D images using *apsum*, adopting an aperture of 10 pixel width (5.8 arcsec). We adopt this value for the aperture to be consistent with Ho et al. (1997), who extracted (red) spectra from an aperture of 4.1 arcsec. The 1D spectra were response-calibrated using the median sensitivity function of each night. After normalization to the flux in the interval 6400-6500 Å the spectra were Doppler shifted to λ_0 : each redshift was taken from NED and then applied to the galaxy spectrum using *dopcor*. For the galaxies observed with both the G7 and G8 grisms, the blue and red spectra were joined using the task *scombine*.

Plots of the nuclear spectra obtained at Loiano are divided among Figures A.1 and A.2 in the Appendix. Out of 19 spectra

Table 1: Continuum correction to $H\alpha$ EW as derived from the color-mass relation of Figure 2.

	$8 \leq M_* \leq 9$	$9 \leq M_* \leq 10$	$10 \leq M_* \leq 11$
$0.8 \leq g-i \leq 1.2$	1.94 ± 0.41	1.91 ± 0.29	1.81 ± 0.24
$0.4 \leq g-i \leq 0.8$	2.43 ± 0.63	2.25 ± 0.45	1.98 ± 0.32
$g-i \leq 0.4$	2.57 ± 0.63	2.48 ± 0.51	-

taken with the G8 grism, 8 can be found in Gavazzi et al. (2011, 2013). The remaining 11 are given in Figure A.2 and are published for the first time in this paper. 25 spectra observed with both the G7 and G8 grisms are shown in Figure A.1 of the appendix.²

The Balmer hydrogen lines are affected by stellar absorption, thus they have been corrected for this effect for proper use in the diagnostic diagrams.

We homogeneously corrected the 26 spectra that we took at Loiano with the G7+G8 grisms, the spectra downloaded from SDSS, the spectra observed by Ho et al. (1997) and the spectra downloaded from the NED database using the GANDALF fitting code (Gas AND Absorption Line Fitting, Sarzi et al. 2006; Falcon-Barroso et al. 2006) complemented by the Penalize Pixel-Fitting code (Cappellari & Emsellem, 2004) to simultaneously model the stellar continuum and the emission lines in individual pixels. Consistently with B15, we used the *MILES* stellar library (Vazdekis et al. 2010). GANDALF is a simultaneous emission and absorption line fitting algorithm designed to separate the relative contribution of the stellar continuum from that of the nebular emission in the spectra of nearby galaxies, while measuring the gas emission and kinematics. This code implements the pPXF method, which combines and adjusts the observed spectra of several stars of all spectral type to the stellar continuum to quantify and remove the underlying absorption. GANDALF was run several times, adjusting the algorithm input parameters, especially on spectra of Ho et al. (1997), because of the presence of the 1000Å gap in these spectra (see section 2 for details).

For the remaining 19 galaxies observed at Loiano with the G8 grism, the insufficient spectral coverage prevents GANDALF from converging. For these galaxies, a statistical absorption correction was applied according to the following procedure. We took a sample of about 5000 galaxies from Consolandi et al. (2016) and constructed their color-stellar mass diagram in Figure 2. For these 5000 galaxies, we downloaded the absorption correction to $H\alpha$ from SDSS (*GalSpecLine*) and constructed a mean correction in nine bins of stellar mass and color (see Table 1) that we applied to the spectra according to each bin of mass and color. The g and i magnitudes for these HRS galaxies were taken from Cortese et al. (2012) and were subsequently corrected for Galactic extinction using the Cardelli et al. (1989) reddening curve; the value of stellar mass is from B15. The resulting $H\alpha$ correction is consistent with the correction obtained using the GANDALF analysis for the individual spectra.

² Actually 26 spectra are shown. The additional, HRS-110, is a combination of a red spectrum taken at Loiano and a spectrum from the SDSS (DR7), whose red part near $H\alpha$ was ruined.

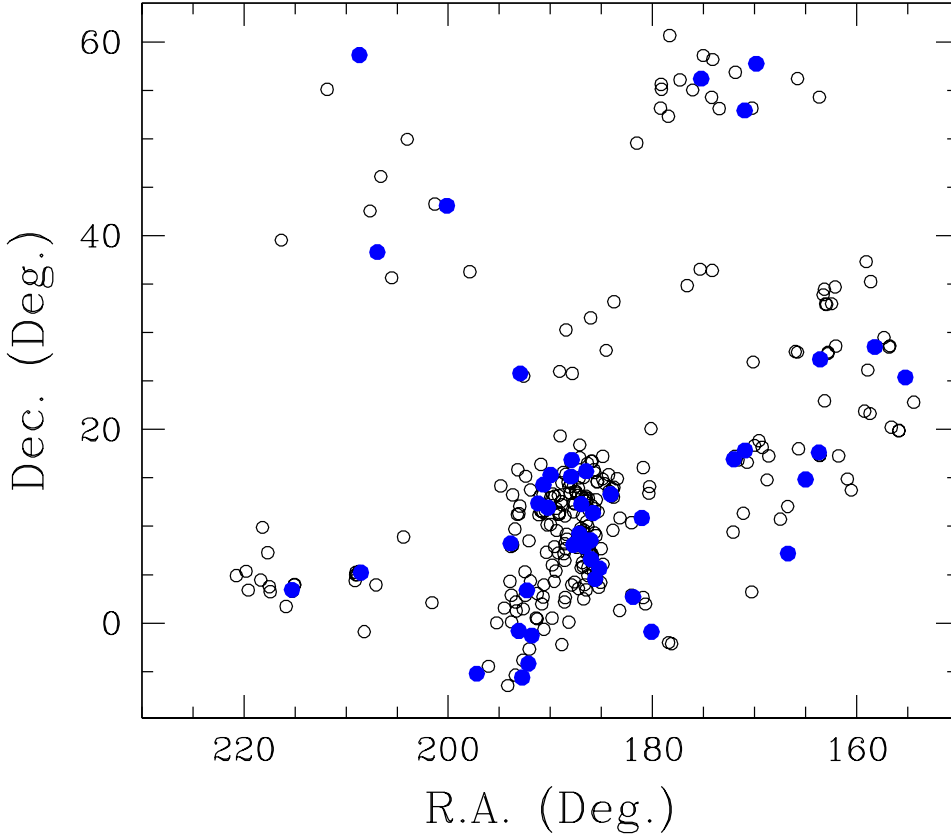


Fig. 1: Sky projection of the full HRS survey (empty symbols) and the subsample of 45 targets whose nuclear spectra were observed with the Cassini Telescope (filled blue).

4. Spectral classification

The determination of the spectral properties of HRS galaxies in this paper is based on four indicators (three versions of the BPT and the WHAN diagram) which exploit the ratio of $[\text{OIII}]/\text{H}\beta$ on $[\text{NII}]/\text{H}\alpha$ or $[\text{SII}]/\text{H}\alpha$ or occasionally on the $[\text{OI}]/\text{H}\alpha$ using the BPT diagnostic diagram, and on the ratio $[\text{NII}]/\text{H}\alpha$ versus the $\text{H}\alpha$ EW, using the WHAN diagram, which holds when the blue emission lines are not available. These diagnostics only classify galaxies with emission lines. Therefore galaxies classified as passive (PAS, showing only absorption lines) or post-starburst (PSB, showing the Balmer series in absorption) have been added a posteriori, by inspecting their spectra by eye. According to Kobulnicky et al. (2003), the ratio of the two adjacent lines can be derived using the equivalent widths instead of the line fluxes.

In order to perform a robust spectral classification, we do not classify integrated and nuclear spectra with signal-to-noise ratio (S/N) of $\text{H}\alpha$ and $\text{H}\beta > 3$. With such a threshold, 48 nuclear spectra (marked with the letter "d" in Table A.4) and 36 integrated spectra (letter "b" in Table A.4) were not classified according to the BPT diagrams. Instead, all nuclear spectra could be classified according to the WHAN diagram and only 8 integrated spectra (marked with letters "b,c" in Table A.4) were excluded from this classification.

In the following spectral analysis we refer always to the LTGs subsample, because their statistic is complete (both nuclear and integrated). As far as concerns the ETGs subsample, 50 integrated spectra were not observed by Boselli et al. (2013): this subsample was not considered in our statistical analysis when we compare the nuclear to the integrated classification. Therefore we refer the reader to a sample of 360 ETGs from the ATLAS3D whose nuclear spectra are given in Gavazzi et al. (2018) for the properties of ETGs.

Figure 3 gives the nuclear classification of HRS galaxies according to the BPT diagnostic diagram based on the $[\text{NII}]/\text{H}\alpha$ ratio (217 objects), on the $[\text{SII}]/\text{H}\alpha$ ratio (217 objects), on the $[\text{OI}]/\text{H}\alpha$ ratio (101 objects) and according to the WHAN diagram (288 objects). Approximately 30 additional galaxies with no emission lines, not included among the 217 nor 288 classified objects, were classified as PAS or PSB.

The region labeled HII (blue) lies to the left of the dotted line defined by K03, while the region occupied by AGNs (red) is to the right of the broken line of Kewley et al. (2001) in both the $[\text{NII}]/\text{H}\alpha$ (first panel) and in the $[\text{OI}]/\text{H}\alpha$ diagrams (third panel). In between the two lines an intermediate region defines the position of the Transition objects (TRAN) (pink). The second panel gives the BPT diagnostic using the ratio $[\text{SII}]/\text{H}\alpha$. Here the straight line (from Kewley et al. 2006) separates Seyfert

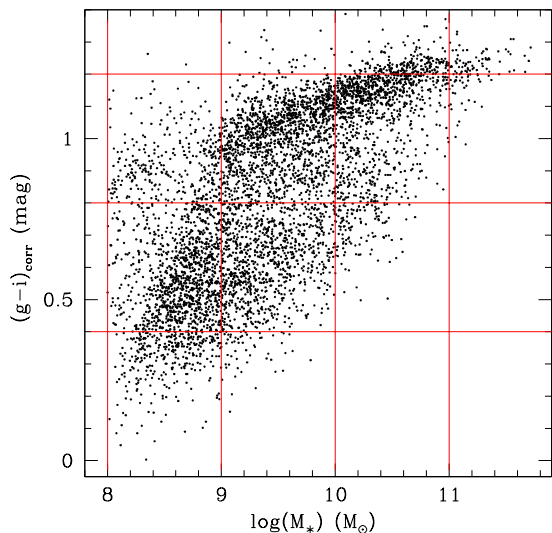


Fig. 2: The color-stellar mass relation for a complete sample of galaxies in the Coma and Local supercluster from Consolandi et al. (2016), subdivided into nine bins of stellar mass and color. In these bins we compute the average SDSS continuum correction to $H\alpha$ (see Table 1).

(SEY, in red) from *LINERs* (LIN, in pink). The fourth panel of Fig. 3 shows the WHAN diagnostic: the different spectral classification and separations between them are from Gavazzi et al. (2011). In this diagram galaxies are divided into five spectral types: HII-regions (blue), sAGN (red), wAGN (pink), RET (green) and PAS.

Using the same diagnostic criteria, Figure 4 gives the BPT and WHAN classifications for integrated spectra with available emission lines, according to the S/N threshold.

In our analysis we refer always to AGNs as TRAN+AGN, LIN+SEY, and sAGN+wAGN. We adopted this definition for the AGNs spectral class to be able to compare our results with those of K03, who defined as AGNs all galaxies beyond the left line in the BPT ($[NII]/H\alpha$) diagram. In specific cases we refer only to “pure” AGNs, namely galaxies above the curve defined by Kewley et al. (2001) in the BPT ($[NII]/H\alpha$) diagram. Also, galaxies classified as PAS or PSB (and RET in the WHAN diagnostic) are always held together.

Despite the different populations and classification criteria, the WHAN and the BPT nuclear diagnostics give consistent results (see Table 2). Hereafter two different percentages are always reported, one is the value resulting from one of the $[NII]/H\alpha$ or $[SII]/H\alpha$ BPT diagrams and the other is from the WHAN diagram. Between 53 and 64% of the nuclear spectra are HII region-like nuclei. The remaining percentage is divided between AGNs (21-27%) and PAS (15-21%). The “pure” AGNs are half of the AGNs percentage: 7-13%. These are galaxies ionized by a SMBH.

Restricting to the 254 LTGs alone, the statistics is altered (see right columns of Table 2): the HII-regions increase to 67-77%; the AGNs become 21-27%; and the PAS spectra decrease to 2-7%. The latter class includes two PSB galaxies: HRS-116 and HRS-195. These two objects show a late-type morphology, with a central bulge and spiral arms, but the SF activity has been stopped suddenly. Also HRS-164 is a LTG with a PAS spectrum: its morphology shows a strong barred structure in the

center, but it is an old and red object.

A comparison between the nuclear and integrated spectral classifications can be performed among the subsample of HRS galaxies with available nuclear and integrated classification (see Fig. 5, Fig. 7, and Fig. 8); the subsample is reported in Table 3. This comparison provides information about how the excitation properties of galaxies change from the center to the outskirts. As can be seen in the three figures, AGNs represent 18-26 % in the nuclear spectra; while in the integrated they decrease to 4-11%. HII-regions are 59-71% in the nuclear classification, becoming 69-84% among the integrated spectra. PAS (including PSB) and RET are 11-15% in the nuclear spectra, becoming 12-20% in the integrated spectra. Altogether, the two diagnostics give consistently that the integrated spectra contain $\sim 10\%$ more HII-region-like spectra than the nuclear ones, together with 10% less AGNs. PAS spectra have an equal frequency: they are 11-15% in the nuclear classification, becoming 12-20% in the integrated one. Figure 6 gives a graphical representation of the migration from nuclear to integrated classification, separately for the various spectral classes. Filled symbols refer to the position of nuclear spectra in the BPT ($[NII]/H\alpha$) diagram, while empty symbols give the position of integrated spectra in the same diagram. Unsurprisingly, only three nuclear AGNs remain AGNs in the integrated classification; all the remaining ones end up as TRAN or HII-regions. All but four nuclear TRAN become HII-regions in the integrated spectra. All but two nuclear HII-regions remain integrated HII-regions. We must highlight that the integrated statistics is biased toward the LTGs, because not all the integrated spectra were taken for the ETGs by Boselli et al. (2013) (only 18/68).

4.1. Mass and environment dependence

Figure 9 shows the distribution of the different nuclear spectral type fractions for HRS late-type galaxies as a function of the stellar mass (from B15) with the respective error bars, computed using the WHAN diagram (left) and the BPT ($[NII]/H\alpha$) diagnostic (right). The number of galaxies in each specific mass bin is reported in parentheses. In spite of the different classification criteria, WHAN and BPT diagrams give consistent dependence of the nuclear spectral properties from stellar mass, excluding PAS spectra because their statistics in the LTG subsample is very small (only 4 objects). As shown in Fig. 9, nuclear HII regions (blue) are exclusively found among galaxies with $M_* \lesssim 10^{9.5} M_\odot$ (90 \pm 9%), and then their fraction decreases with increasing stellar mass. On the contrary, the frequency of AGNs (red) (including TRAN, black) is low, at $M_* \lesssim 10^{9.5} M_\odot$ (8 \pm 2%) and increases significantly with stellar mass, reaching 66 \pm 14% above $10^{10.0} M_\odot$, suggesting that approximately two thirds of the late-type galaxies in the local Universe, at that stellar mass value, contain an AGN or at least a TRAN object.

This also suggests that there is a clear dependency of the nuclear ionization source from galaxy stellar mass: less-massive galaxies are more likely to contain a nucleus ionized by young stellar population, compared to more-massive galaxies, which contain an AGN or a TRAN object.

Moreover previous works, such as K03, demonstrate that the AGNs fraction continues to grow at higher stellar mass. We conclude that even on nuclear scales, LTG galaxies suffer from decreasing SFR with increasing mass, a “downsizing” behavior, reinforcing the early claim by Gavazzi et al. (1996).

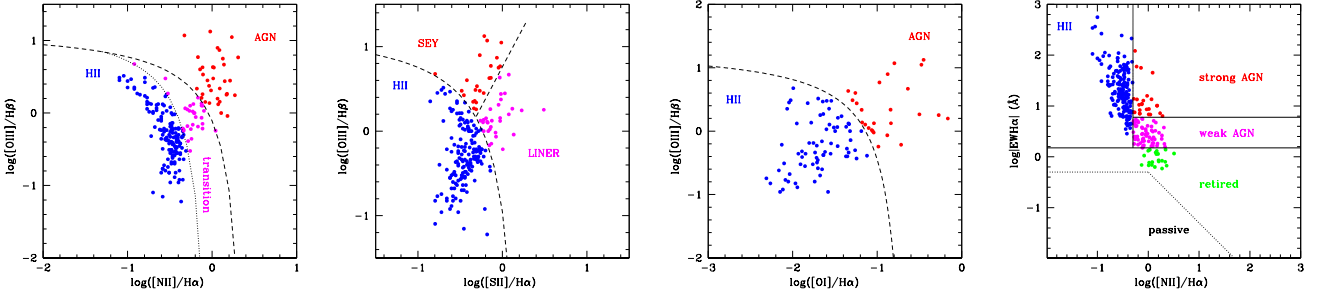


Fig. 3: Nuclear diagnostic diagrams for the whole HRS sample limited to emission-line objects with S/N ratio $\zeta \geq 3$. In the left BPT diagram the broken separation line between AGNs (red) and TRAN (pink) galaxies is from Kewley et al. (2001), while the dotted separation line between TRAN (pink) and HII region-like nuclei (blue) is from K03. In the second BPT diagram the extreme starburst classification line is from Kewley et al. (2001), while the separation between LINER (pink) and SEY (red) is from Kewley et al. (2006). We note that the pink filled symbols refer to different types of objects in the three diagrams. The third panel reports the BPT diagram for the minority of galaxies (101) with [OI] in emission. In the WHAN diagram the separations between the different classes are from Gavazzi et al. (2011).

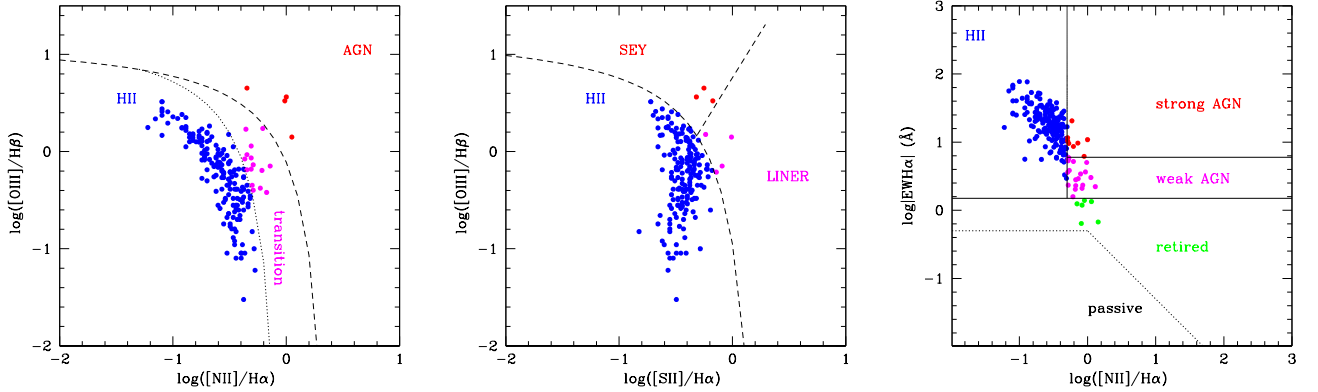


Fig. 4: Integrated diagnostic diagrams for emission-line objects with S/N ratio $\zeta \geq 3$. Broken separations in the diagrams are the same as in Fig. 3.

Table 2: The frequency of the different types of nuclear spectra in the whole HRS sample (left) and among the 254 LTGs (right), including galaxies a posteriori classified as passive or post-starburst.

BPT ([NII]/H α) 255/322	AGN 34 (13%) TRAN 31 (12%) HII 152 (60%) PAS 36 (14%) PSB 2 (1%)	BPT ([NII]/H α) 206/254	AGN 26 (13%) TRAN 27 (13%) HII 149 (72%) PAS 2 (1%) PSB 2 (1%)
BPT ([SII]/H α) 255/322	SEY 23 (9%) LIN 30 (12%) HII 164 (64%) PAS 36 (14%) PSB 2 (1%)	BPT ([SII]/H α) 206/254	SEY 20 (10%) LIN 24 (11%) HII 158 (77%) PAS 2 (1%) PSB 2 (1%)
WHAN 322/322	sAGN 24 (7%) wAGN 63 (20%) HII 171 (53%) RET 28 (9%) PAS 34 (11%) PSB 2 (1%)	WHAN 254/254	sAGN 21 (8%) wAGN 47 (19%) HII 168 (67%) RET 14 (6%) PAS 2 (0.5%) PSB 2 (0.5%)

4.2. Star formation: the Brinchmann 04 program

Understanding the physical processes that drive SF and the rate at which galaxies form stars is crucial for the study of galaxy evolution. In recent decades, the available multiwavelength observations, from X-rays to radio bands, have been used to define a set of SF indicators. The most frequently used are: the UV continuum, nebular recombination lines (primarily H α), far-IR

dust emission, and the synchrotron radio continuum at 21 cm (Kennicutt 1983). Only the comparison of two or more SF indicators provides reliable measure of the SFR in galaxies.

Many works in the literature proposed to compute the SFR directly from nuclear spectroscopy. Whether or not the global SF properties of nearby galaxies can be extrapolated from the available SDSS fiber spectroscopy (*aperture correction problem*) is

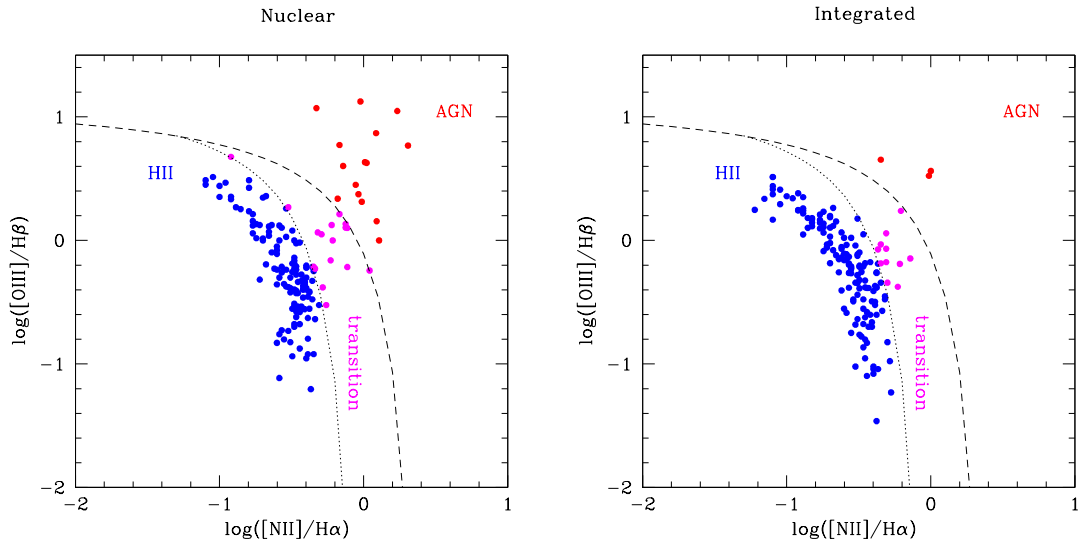
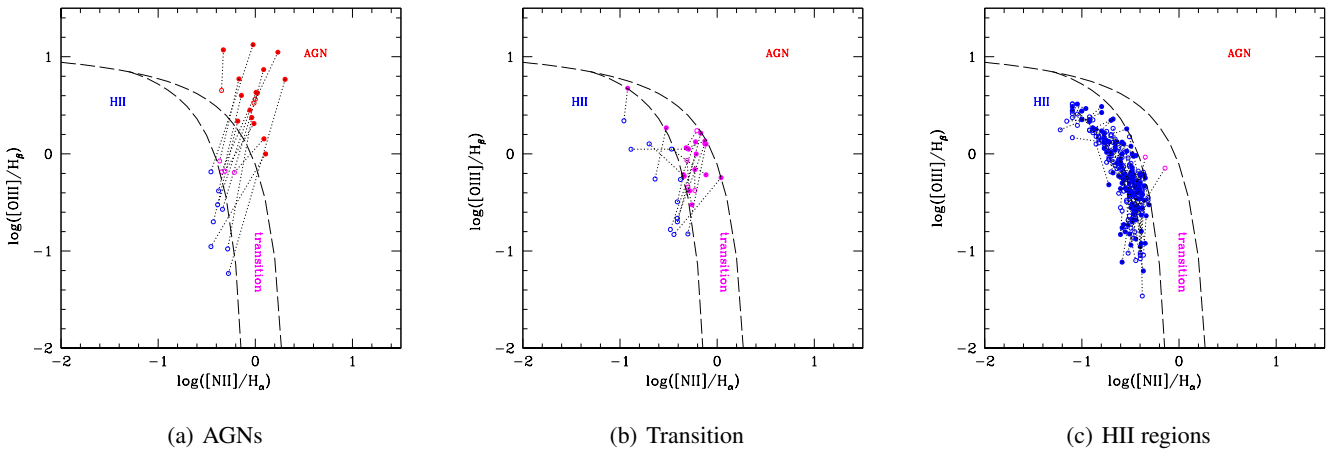


Fig. 5: BPT diagrams for 164 HRS objects that have both the nuclear and integrated classification available in the $[OIII]/H\beta$ vs. $[NII]/H\alpha$ diagram. The separation lines are the same as in Figure 3.



(a) AGNs (b) Transition (c) HII regions
Fig. 6: Migration from nuclear (filled symbols) to integrated (empty symbols) in the *BPT* diagram.

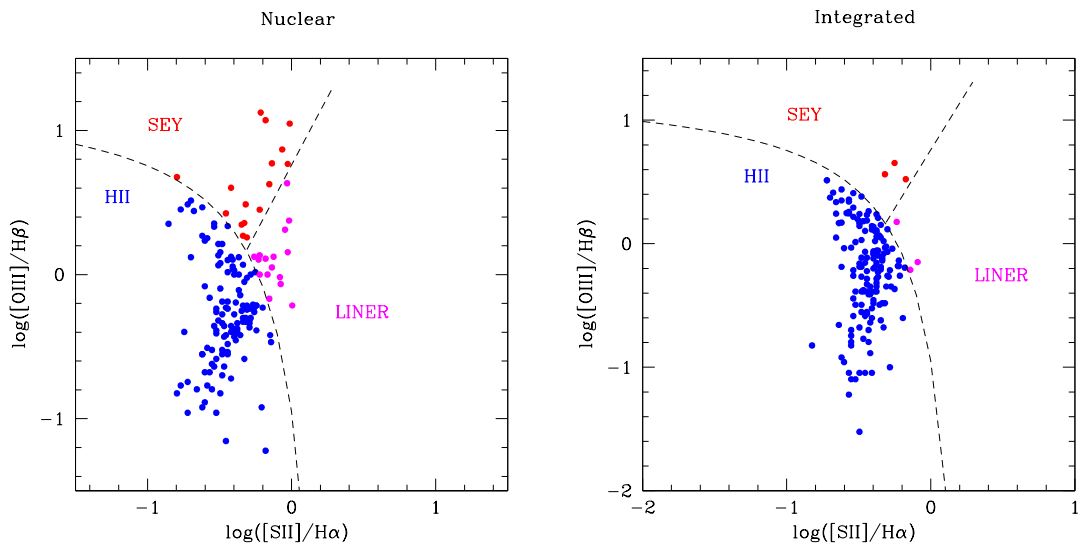


Fig. 7: BPT diagrams for 164 galaxies that have the ratios $[OIII]/H\beta$ and $[SII]/H\alpha$ available both from the nuclear and integrated spectra. The dotted separation lines are the same as in Figure 3.

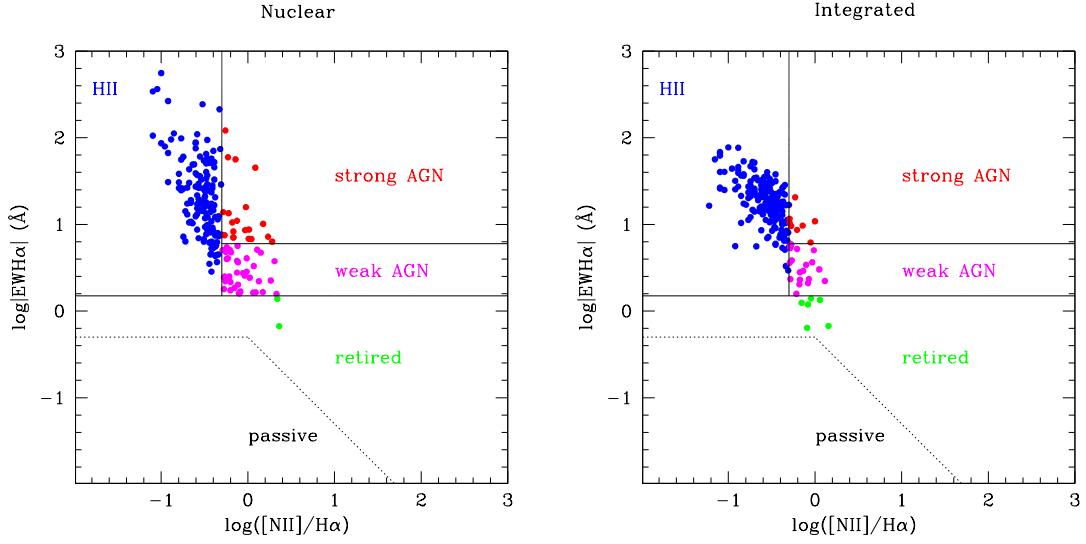


Fig. 8: WHAN diagrams for 244 galaxies with the ratios $[NII]/H\alpha$ and $H\alpha$ EW available both from nuclear and integrated spectra. The separations are the same as in Figure 3.

Table 3: Statistics of integrated and nuclear spectra for HRS galaxies with line ratios available both from the nuclear and integrated spectra, including galaxies a posteriori classified as passive or post-starburst.

	Nuclear	Integrated
BPT ($[NII]/H\alpha$) 185/322	AGN 15 (8%) TRAN 20 (11%) HII 129 (70%) PAS 19 (10%) PSB 2 (1%)	AGN 3 (2%) TRAN 11 (6%) HII 148 (79%) PAS 23 (13%)
BPT ($[SII]/H\alpha$) 185/322	SEY 16 (9%) LIN 16 (9%) HII 132 (71%) PAS 19 (10%) PSB 2 (1%)	SEY 3 (2%) LIN 3 (2%) HII 156 (84%) PAS 23 (12%)
WHAN 264/322	sAGN 22 (8%) wAGN 46 (18%) HII 155 (59%) RET 20 (7%) PAS 18 (7%) PSB 2 (1%)	sAGN 8 (3%) wAGN 20 (8%) HII 182 (69%) RET 21 (8%) PAS 32 (12%)

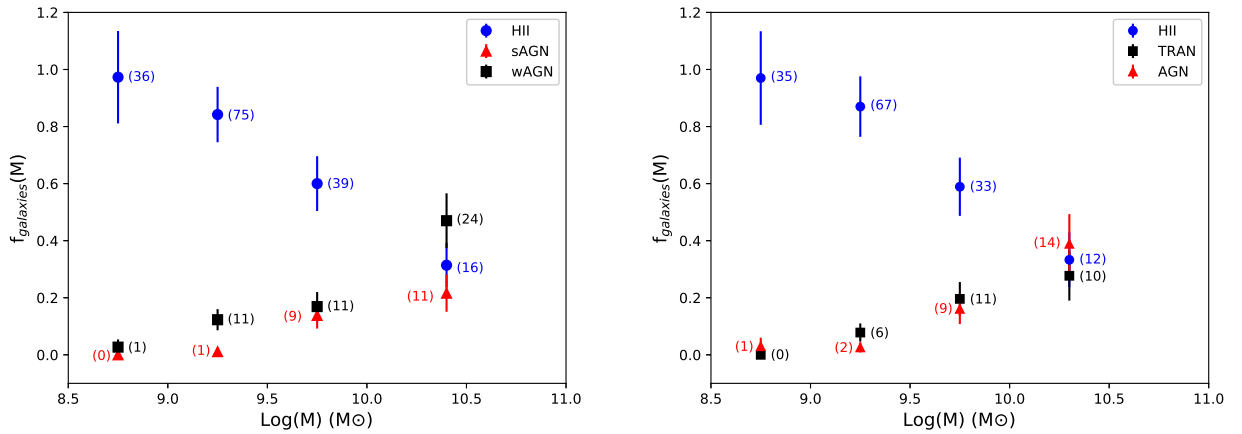


Fig. 9: Distribution of nuclear spectral type fractions for LTGs as a function of the stellar mass, using the classification provided by the WHAN (left) and by the BPT ($[NII]/H\alpha$) (right) diagram.

still debated.

In this section, we test for the HRS galaxies the global SFR derived by B04 from SDSS nuclear spectra with the $H\alpha$ -derived SFR of B15. B04 proposed a method to extrapolate the global SFR of local galaxies from SDSS nuclear spectra using aperture correction based on photometric optical colors. Summarizing, B04 computed the SFR of AGNs and TRAN objects from the 4000 Å break and for HII-regions from a global emission-line estimate obtained by fitting Charlot & Longhetti (2001) models to the nuclear spectra for galaxies belonging to the SDSS database. These values were corrected using an estimate of the external color of galaxies derived from the difference in color between the *cModel* magnitude (the magnitude based on the best-fitting of the exponential and de Vaucouleurs models in the *r* band, Abazajian et al. 2004) and the *fiber* magnitude (the magnitude in 3-arcsec-diameter SDSS fiber radius). The global SFR is obtained by adding the external to the nuclear SFR. Both the stellar mass and SFR in B04 are computed assuming a Kroupa (2001) IMF. B04 data are available through the SDSS database (*galSpecExtra* table) for 205186 galaxies with $z \lesssim 0.1$ in the sky region corresponding to the one covered by the HRS. Figure 10 represents the relation between the stellar mass and the $\log(\text{SFR}_{\text{total}})$ for the aforementioned SDSS galaxies (see contours). The appearance of the galaxy main sequence is evident, separated by a cloud of quenched galaxies, a factor of one hundred less star forming.

Among galaxies listed in *galSpecExtra* we found the data for 38 HRS galaxies. For these we plot the value derived by B04 with open symbols. Conversely the filled symbols represent the SFR obtained by B15 directly from the $H\alpha$ integrated photometry (corrected to transform from Salpeter 1955 to Kroupa 2001 IMF). The filled symbols precisely overlap the galaxies SF main sequence (SFMS). On the contrary, most B04 SFR estimates are at least a factor of one hundred less than the actual integrated values. In particular, for three galaxies, the B04 value is smaller by a factor of one hundred; for eight galaxies, the B04 value is smaller by a factor of between ten and one hundred. The logarithmic mean deviation between B04 and B15 SFR estimations is 0.7. However we must highlight that the B04 study includes SDSS galaxies with $0.005 < z < 0.22$, while the HRS comprises galaxies with $cz < 3000 \text{ km s}^{-1}$, therefore suffering from more severe aperture correction than B04.

5. Discussion and conclusions

In this paper we have used the BPT and the WHAN diagnostic diagrams to derive the nuclear spectral classification of galaxies belonging to the HRS, a statistically representative magnitude and volume limited sample of 322 local galaxies, spanning a wide range in morphology and stellar mass, and belonging to different environments. The determination of the relative frequency of AGNs versus other spectral classes, for example, HII region-like, PAS, and RET, in a statistically complete sample of local galaxies is important to discriminate the source of ionization in the nuclear region of galaxies (e.g., black holes vs. young or old stars).

We present new nuclear long-slit spectroscopy of 45 HRS galaxies, which, added to the ones available from the literature, gives a complete nuclear spectroscopic census of all HRS galaxies more massive than $10^{8.5} M_{\odot}$. The completeness of the observations allows us to make a statistical analysis of the spectroscopic nuclear properties of this sample.

We note that, after checking that using different diagnostics does not change the global statistics, we separated the different spec-

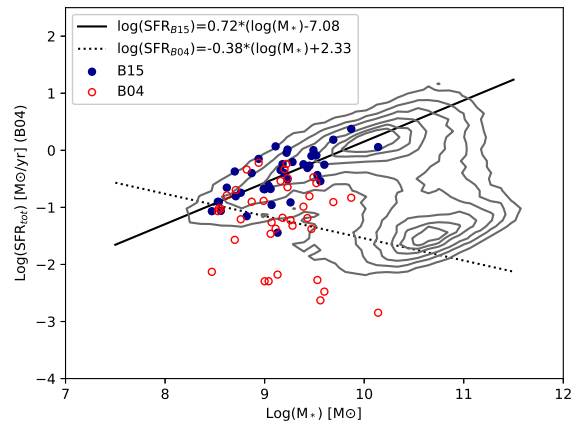


Fig. 10: The relation between the stellar mass and the global SFR as computed by B04 (contours). Open symbols represent 38 HRS galaxies computed by B04 (dotted line represents the best fit to these data), while filled symbols are the integrated SFR derived for them by B15 using $H\alpha$ integrated photometry (solid line is the best fit to these data). The filled symbols precisely overlap the SFMS of galaxies in the local Universe; instead the value of SFR estimated by B04 is underestimated and does not follow the SFMS trend.

tral classes by means of only the BPT(NII/H α). We separated AGNs from HII and TRAN objects following the prescriptions of Kewley et al. (2001) and K03. Our main results can be summarized as follow:

- 1) As for the whole HRS sample about half of the nuclear spectra (53-64%) are HII region-like nuclei, while AGNs (including TRAN) represent 21-27% and PAS (including RET) spectra make up 15-21%. Restricting to the 254 LTGs, the percentage of AGNs+TRAN varies between 22% and 27%, the fraction of HII-regions increases to 67-77%, and PAS (including RET) spectra represent a mere 1-7%. However, the classification schemes provided by the various diagnostics cannot be fully reconciled: for example, the class "Transition" exists only in the classic BPT diagram, and the division between strong and weak AGNs is provided only by the WHAN diagram; the same applies to the classification of retired galaxies (that were identified by Cid Fernandez et al. (2011) as presently inactive nuclei, previously ionized by post-AGB stars). Moreover, the scatter between the various classifications appears large, as it was also concluded, in particular for LINERs, by Balmaverde & Capetti (2014) who compared HST high spatial- and spectral-resolution observations of low-luminosity AGNs with ground-based lower-resolution spectra. To reduce as much as possible the inconsistencies of the individual spectral classification schemes, we evaluate the *mode* between the four classifications in Figure 3. In order to find a criterion for reliable classification, we select all galaxies whose *mode* is consistently provided by at least three methods (we note that spectra in which emission lines are absent, no matter if they were considered RET in the WHAN, PSB (poststarburst) or purely passive (PAS), were reclassified by hand as PAS, and therefore their *mode* classification is PAS with four votes). In the end, 195 targets out of 264 LTG galaxies have their *mode* composed of three coherent classifications. In order to study a possible environmental dependence of these frequencies we plot the mass distributions of the spectral fractions in Fig.

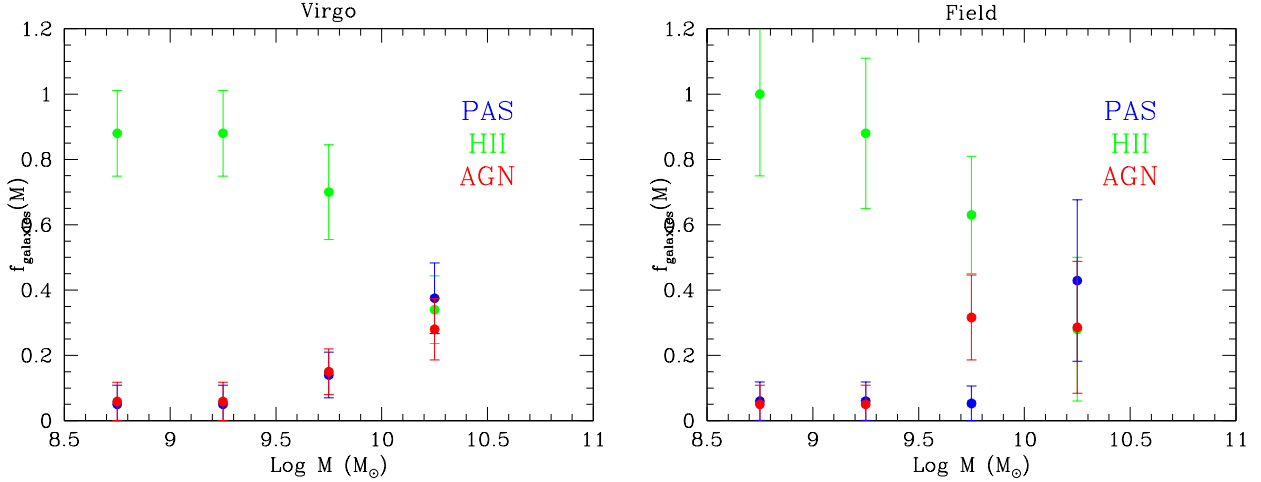


Fig. 11: Mass distributions of the *mode* of four different nuclear spectral classifications for the late-type HRS galaxies inside the Virgo cluster (left) and outside it (right).

11, separately inside (left panel) and outside (right panel) the Virgo cluster (projected distance from M87 equal to two virial radii, assuming that the virial radius of the Virgo cluster is 1.7 Mpc from Boselli & Gavazzi 2006). From Fig. 11 it is clear that the dependency of the nuclear spectral types on galaxy stellar mass remain visible also observing galaxies in different environments. However, no significant environmental dependence is found for the AGN frequency: among galaxies with $M_* \geq 10^{10.0} M_\odot$ they are consistent with $30 \pm 7\%$ inside or outside the Virgo cluster. In both environments the decrease of the frequency of HII region-like nuclei with increasing stellar mass is compensated by a combined increase of the fraction of AGNs and of passive nuclei (including those previously classified as RET that are known to derive from post AGB stars).

2) Regarding the comparison between the nuclear and the integrated classification, as expected, the fraction of AGNs+TRAN integrated spectra is significantly lower than in the nuclei; they are only 4-11% instead of 18-26% ($\sim 10\%$ lower). This decrease is compensated by an equal increase of HII region-like spectra (from 59-71% in the nuclear to 69-84% in the integrated classification). There is no significant change from the nuclear to the integrated classification in the percentage of PAS (including RET) spectra. This confirms previous results by Moustakas et al. (2006, 2010) and Iglesias-Páramo et al. (2013, 2016) who found that the relative fraction of star-forming galaxies versus AGNs is a strong function of the integrated light enclosed by the spectroscopic aperture. Iglesias-Páramo et al. (2013, 2016) observed 104 spiral galaxies in the CALIFA survey with an IFS, finding that the $H\alpha$ flux and the $H\alpha$ EW increase from the nucleus to the outer regions of galaxies with no dependence on galaxy inclination and stellar mass. Furthermore, Moustakas et al. (2010) provided optical nuclear, circumnuclear, and semi-integrated spectra of 65 galaxies in SINGS (Kennicutt et al. 2003), finding that the fraction of the sample classified as AGNs decreases by $\sim 30\%$ as the light fraction increases by $\sim 50\%$, with a corresponding increase in the fraction of galaxies classified as HII-regions. Finally, Belfiore et al. (2016), who

studied the spatially resolved excitation properties of the ionized gas for 646 galaxies belonging to SDSS-IV MaNGA, concluded that the excitation properties of galaxies change from the center to the outskirts in a very complex way. As the coverage of ETGs in the HRS is incomplete, we refer the reader to Gavazzi et al. (2018) who analyze the nuclear properties of a sample of 360 ETGs from the ATLAS3D.

3) Restricting to the 254 LTGs, we computed the spectral classes distribution as a function of stellar mass. The percentage of HII regions is inversely proportional to the stellar mass (90% for galaxies with $M_* \leq 10^{9.5} M_\odot$) while that of AGNs (including TRAN) is directly proportional. We find that approximately two thirds (66%) of spiral galaxies in the local Universe ($z \leq 0.03$) with $\leq M_* \leq 10^{10.0} M_\odot$ contain an AGN or a TRAN object, that is, a nucleus not ionized by a young stellar population (O and B stars), but ionized by a supermassive black hole or old post-AGB stars. Our result is consistent with K03 who examined the properties of the host galaxies of 22623 AGNs with $0.02 \leq z \leq 0.3$ selected from the SDSS. First of all, we note that K03 defines AGNs as all galaxies that lie to the right of the line defined by K03 in the BPT diagram, so we can compare our results on AGNs+TRAN to these. K03 found that AGNs reside almost exclusively in massive galaxies: between $3 \times 10^{10} M_\odot$ and $10^{11} M_\odot$, they represent 50% at very low redshift ($z \sim 0.02$). More recently, Sanchez et al. (2017) remarks that AGNs are hosted in the most massive galaxies, namely mostly ETGs or early-type spirals, with an important bulge.

4) Restricting to the 254 LTGs we also computed the spectral type distribution as a function of environment, considering that 148 HRS galaxies belong to the Virgo cluster. No significant environmental dependence is found for AGNs (including TRAN): for galaxies with $M_* \geq 10^{9.0} M_\odot$ they are consistent with $\sim 33\%$ inside the Virgo cluster and with $\sim 30\%$ outside it. Similar results are obtained restricting to the "pure" AGNs, at the same stellar mass; they reach $\sim 13\%$ inside the Virgo cluster and $\sim 14\%$ outside it. These results suggest that AGNs, including or ex-

cluding TRAN objects, exist with similar frequencies in clusters and in the field. Both inside and outside Virgo, the frequency of AGNs found in this work is higher than the percentage found by Marziani et al. (2017) in the WINGS survey (Fasano et al. 2006) and by B04 in the SDSS. However, after inspection of the individual AGN spectra in this work (prior and after the GANDALF correction) we found that the classification of 4 out of 26 AGN spectra is highly uncertain, making the above difference insignificant.

5) B15 computed the SFR for the HRS galaxies. Thirty-eight of these are also part of B04. The SFR derived from the global measurements (both spectroscopic and imaging) for this set of 38 HRS galaxies is inconsistent with the value obtained by B04 with his aperture-corrected method: the former being in most cases two orders of magnitude larger than the values of B04. This confirms previous results by Richards et al. (2015) who tested the B04 method for 1212 galaxies belonging to the SAMI Galaxy survey (Croom et al. 2012). Richards et al. (2015) conclude that the nuclear spectrum is not representative of the properties of the entire galaxy, mainly because of the different dust content: $H\alpha/H\beta$ ratio (extinction) decreases from the center towards larger radii; therefore, galaxies with different morphology require different dust attenuation corrections. Similar results have been obtained by Iglesias-Páramo et al. (2013) who confirmed that local star-forming galaxies observed through a small aperture are misclassified as quiescent if the aperture-correction method is based only on the nuclear properties, because the fraction of a galaxy covered by a fixed aperture varies with redshift. We maintain that the B04 aperture-correction method does not provide a robust extrapolation of the global SFR for local galaxies ($z \lesssim 0.03$).

Acknowledgements. This research has made use of the GOLDmine database (Gavazzi et al. 2003, 2014b) and of the NASA/IPAC Extragalactic Database (NED) which is operated by the Jet Propulsion Laboratory, California Institute of Technology, under contract with the National Aeronautics and Space Administration. Funding for the Sloan Digital Sky Survey (SDSS) and SDSS-II has been provided by the Alfred P. Sloan Foundation, the Participating Institutions, the National Science Foundation, the U.S. Department of Energy, the National Aeronautics and Space Administration, the Japanese Monbukagakusho, and the Max Planck Society, and the Higher Education Funding Council for England. The SDSS Web site is <http://www.sdss.org/>. The SDSS is managed by the Astrophysical Research Consortium (ARC) for the Participating Institutions. The Participating Institutions are the American Museum of Natural History, Astrophysical Institute Potsdam, University of Basel, University of Cambridge, Case Western Reserve University, The University of Chicago, Drexel University, Fermilab, the Institute for Advanced Study, the Japan Participation Group, The Johns Hopkins University, the Joint Institute for Nuclear Astrophysics, the Kavli Institute for Particle Astrophysics and Cosmology, the Korean Scientist Group, the Chinese Academy of Sciences (LAMOST), Los Alamos National Laboratory, the Max-Planck-Institute for Astronomy (MPIA), the Max-Planck-Institute for Astrophysics (MPA), New Mexico State University, Ohio State University, University of Pittsburgh, University of Portsmouth, Princeton University, the United States Naval Observatory, and the University of Washington.

References

Abazajian, K. N., Adelman-McCarthy, J. K., Agüeros, M. A., et al. 2009, *ApJS*, 182, 543-558
 Abazajian, K., Adelman-McCarthy, J. K., Agüeros, M. A., et al. 2004, *AJ*, 128, 502
 Alam, S., Albareti, F. D., Allende Prieto, C., et al. 2015, *ApJS*, 219, 12
 Albareti, F. D., et al. 2016, [arXiv:1608.02013](https://arxiv.org/abs/1608.02013)
 Baldwin, J. A., Phillips, M. M., & Terlevich, R. 1981, *PASP*, 93, 5
 Balmaverde, B., & Capetti, A. 2014, *A&A*, 563, A119
 Bassett, R., Glazebrook, K., Fisher, D. B., et al. 2017, *MNRAS*, 467, 239
 Belfiore, F., Maiolino, R., Maraston, C., et al. 2016, *MNRAS*, 461, 3111
 Belfiore, F., Maiolino, R., Tremonti, C., et al. 2017, *MNRAS*, 469, 151
 Bendo, G. J., Galliano, F., & Madden, S. C. 2012, *MNRAS*, 423, 197

Boquien, M., Boselli, A., Buat, V., et al. 2013, *A&A*, 554, A14
 Boselli, A., & Gavazzi, G. 2002, *A&A*, 386, 124
 Boselli, A., & Gavazzi, G. 2006, *PASP*, 118, 517
 Boselli, A., Eales, S., Cortese, L., et al. 2010, *PASP*, 122, 261
 Boselli, A., Ciesla, L., Cortese, L., et al. 2012, *A&A*, 540, A54
 Boselli, A., Hughes, T. M., Cortese, L., Gavazzi, G., & Buat, V. 2013, *A&A*, 550, A114
 Boselli, A., & Gavazzi, G. 2014, *A&A Rev.*, 22, 74
 Boselli, A., Cortese, L., & Boquien, M. 2014, *A&A*, 564, A65
 Boselli, A., Cortese, L., Boquien, M., et al. 2014, *A&A*, 564, A66
 Boselli, A., Cortese, L., Boquien, M., et al. 2014, *A&A*, 564, A67
 Boselli, A., Fossati, M., Gavazzi, G., et al. 2015, *A&A*, 579, A102
 Brinchmann, J., Charlot, S., White, S. D. M., et al. 2004, *MNRAS*, 351, 1151
 Bruzual, G., & Charlot, S. 2003, *MNRAS*, 344, 1000
 Capetti, A., & Baldi, R. D. 2011, *A&A*, 529, A126
 Cappellari, M., & Emsellem, E. 2004, *PASP*, 116, 138
 Cappellari, M. 2017, *MNRAS*, 466, 798
 Cardelli, J. A., Clayton, G. C., & Mathis, J. S. 1989, *ApJ*, 345, 245
 Cattaneo, A., Blaizot, J., Devriendt, J. E. G., et al. 2017, *MNRAS*, 471, 1401
 Charlot, S., & Longhetti, M. 2001, *MNRAS*, 323, 887
 Charlot, S., Kauffmann, G., Longhetti, M., et al. 2002, *MNRAS*, 330, 876
 Cid Fernandes, R., Stasińska, G., Mateus, A., & Vale Asari, N. 2011, *MNRAS*, 413, 1687
 Ciesla, L., Boselli, A., Smith, M. W. L., et al. 2012, *A&A*, 543, A161
 Ciesla, L., Boselli, A., Smith, M. W. L., et al. 2013, *A&A*, 550, C1
 Ciesla, L., Boquien, M., Boselli, A., et al. 2014, *A&A*, 565, A128
 Ciesla, L., Boselli, A., Elbaz, D., et al. 2016, *A&A*, 585, A43
 Consolandi, G., Gavazzi, G., Fumagalli, M., Dotti, M., & Fossati, M. 2016, *A&A*, 591, A38
 Cortese, L., Boissier, S., Boselli, A., et al. 2012, *A&A*, 544, A101
 Cortese, L., Fritz, J., Bianchi, S., et al. 2014, *MNRAS*, 440, 942
 Falco, E. E., Kurtz, M. J., Geller, M. J., et al. 1999, *PASP*, 111, 438
 Falcón-Barroso, J., Bacon, R., Bureau, M., et al. 2006, *MNRAS*, 369, 529
 Fasano, G., Marmo, C., Varela, J., et al. 2006, *A&A*, 445, 805
 Fontanot, F., De Lucia, G., Hirschmann, M., et al. 2017, *MNRAS*, 464, 3812
 Fossati, M., Wilman, D. J., Mendel, J. T., et al. 2017, *ApJ*, 835, 153
 Gavazzi, G., Pierini, D., & Boselli, A. 1996, *A&A*, 312, 397
 Gavazzi, G., Zaccardo, A., Sanvito, G., Boselli, A., & Bonfanti, C. 2004, *A&A*, 417, 499
 Gavazzi, G., Savorgnan, G., & Fumagalli, M. 2011, *A&A*, 534, A31
 Gavazzi, G., Consolandi, G., Dotti, M., et al. 2013, *A&A*, 558, A68
 Gavazzi, G., Pedraglio, S., Consolandi, G., et al. 2017, *A&A*, submitted
 Gavazzi, G., & Boselli, A. 1999, *A&A*, 343, 86
 Gualandi, R., & Merighi, R. Technical report 2001, Bologna Astronomical Observatory
 Heckman, T. M. 1980, *A&A*, 87, 152
 Ho, L. C., Filippenko, A. V., & Sargent, W. L. 1995, *ApJS*, 98, 477
 Ho, L. C., Filippenko, A. V., & Sargent, W. L. W. 1997, *ApJS*, 112, 315
 Hughes, T. M., Cortese, L., Boselli, A., Gavazzi, G., & Davies, J. I. 2013, *A&A*, 550, A115
 Iglesias-Páramo, J., Vílchez, J. M., Galbany, L., et al. 2013, *A&A*, 553, L7
 Iglesias-Páramo, J., Vílchez, J. M., Rosales-Ortega, F. F., et al. 2016, *ApJ*, 826, 71
 Jansen, R. A., Fabricant, D., Franx, M., & Caldwell, N. 2000, *ApJS*, 126, 331
 Jones, D. H., Read, M. A., Saunders, W., et al. 2009, *MNRAS*, 399, 683
 Kauffmann, G., White, S. D. M., & Guiderdoni, B. 1993, *MNRAS*, 264, 201
 Kauffmann, G., Heckman, T. M., White, S. D. M., et al. 2003, *MNRAS*, 341, 54
 Kauffmann, G., Heckman, T. M., Tremonti, C., et al. 2003b, *MNRAS*, 346, 1055
 Kennicutt, R. C., Jr. 1992, *ApJ*, 388, 310
 Kennicutt, R. C., Jr. 1998, *ARA&A*, 36, 189
 Kennicutt, R. C., Jr., Armus, L., Bendo, G., et al. 2003, *PASP*, 115, 928
 Kennicutt, R. C., Calzetti, D., Aniano, G., et al. 2011, *PASP*, 123, 1347
 Kewley, L. J., Dopita, M. A., Sutherland, R. S., Heisler, C. A., & Trevena, J. 2001, *ApJ*, 556, 121
 Kewley, L. J., Groves, B., Kauffmann, G., & Heckman, T. 2006, *MNRAS*, 372, 961
 Kobulnicky, H. A., & Phillips, A. C. 2003, *ApJ*, 599, 1031
 Kroupa, P. 2001, *MNRAS*, 322, 231
 Lagos, C. d. P., Theuns, T., Schaye, J., et al. 2016, *MNRAS*, 459, 2632
 Maraston, C., & Strömbäck, G. 2011, *MNRAS*, 418, 2785
 Marziani, P., D'Onofrio, M., Bettoni, D., et al. 2017, *A&A*, 599, A83
 Massey, P., Strobel, K., Barnes, J. V., & Anderson, E. 1988, *ApJ*, 328, 315
 Richards, S. N., Bryant, J. J., Croom, S. M., et al. 2016, *MNRAS*, 455, 2826
 Moustakas, J., & Kennicutt, R. C., Jr. 2006, *ApJ*, 651, 155
 Moustakas, J., Kennicutt, R. C., Jr., Tremonti, C. A., et al. 2010, *ApJS*, 190, 233-266
 Poggianti, B. M., Jaffé, Y. L., Moretti, A., et al. 2017, *Nature*, 548, 304
 Salpeter, E. E. 1955, *ApJ*, 121, 161

- Sánchez, S. F., Kennicutt, R. C., Gil de Paz, A., et al. 2012, *A&A*, 538, A8
Sanchez, S. F., Avila-Reese, V., Hernandez-Toledo, H., et al. 2017, arXiv:1709.05438
Sánchez, S. F., García-Benito, R., Zibetti, S., et al. 2016, *A&A*, 594, A36
Sarzi, M., Falcón-Barroso, J., Davies, R. L., et al. 2006, *MNRAS*, 366, 1151
Schreiber, C., Elbaz, D., Pannella, M., et al. 2016, *A&A*, 589, A35
Tremonti, C. A., Heckman, T. M., Kauffmann, G., et al. 2004, *ApJ*, 613, 898
Vazdekis, A., Sánchez-Blázquez, P., Falcón-Barroso, J., et al. 2010, *MNRAS*, 404, 1639
Veilleux, S., Kim, D.-C., Sanders, D. B., Mazzarella, J. M., & Soifer, B. T. 1995, *ApJS*, 98, 171
York, D. G., Adelman, J., Anderson, J. E., Jr., et al. 2000, *AJ*, 120, 1579
Zibetti, S., Charlot, S., & Rix, H.-W. 2009, *MNRAS*, 400, 1181

Appendix A: Tables description

Here we report the description of the observations at the Cassini telescope and the three tables which include our results. The observing log of 45 galaxies whose nuclear spectra were taken at Loiano is given in Table A.1

The spectroscopic parameters of HRS galaxies observed at Loiano only with the red-channel grism are given in Table A.2

The spectroscopic parameters of 25 HRS galaxies observed at Loiano with the red and blue-channel grism are given in Table A.3

The spectroscopic parameters derived for all HRS galaxies are given in Table A.4

HRS	Alpha	Delta	PA	Blue			Red		
				Obs date	Ncomb	expT	Obs date	Ncomb	expT
(1)	hhmmss.ss	ddppss.s	deg	yyyy-mm-dd	(6)	sec	yyyy-mm-dd	(9)	sec
(2)	(3)	(4)	(5)	(6)	(7)	(8)	(9)	(10)	
2*	102057.13	+252153.4	30	2017-04-20	3	480	2013-2017	6	300
9	103255.45	+283042.2	90				2015-03-20	3	180
28*	105420.89	+271423.1	90	2017-04-21	3	480	2009-2017	9	300
32*	105448.63	+173716.4	90				2009-2013	6	300
33*	110002.38	+145029.7	90	2017-04-21	3	480	2009-2017	15	300
38*	110656.63	+071026.1	90				2009-2013	9	240
45	111921.60	+574527.8	90				2015-03-23	4	180
51*	112345.53	+174907.2	90	2017-04-20	3	480	2009-2017	3	300
52*	112355.58	+525515.6	90				2009-2013	9	180
58	112809.41	+165513.7	90				2015-03-23	6	300
65*	114053.42	+561207.3	87	2017-05-25	3	600	2013-2017	6	300
77*	120023.63	-010600.3	90				2012-03-15	3	360
84	120411.55	+105115.8	59				2015-03-20	6	300
86*	120737.15	+024125.8	140	2017-04-20	3	480	2009-2017	6	300
98*	121622.52	+131825.4	57	2017-05-25	3	600	2012-2013	6	300
108*	122048.49	+053823.6	74	2017-05-26	3	600	2009-2013	10	300
110*	122117.79	+113040.0	145	SDSS DR7			2012-03-16	3	300
118	122227.25	+043358.7	55	2017-04-20	3	600	2015-2017	6	360
124	122317.25	+112204.7	58				2015-03-23	3	300
132	122407.44	+063626.9	90	2017-04-21	3	600	2015-2017	6	300
134*	122414.53	+083209.1	90				2013-03-12	3	120
148	122558.80	+154017.3	134	2017-04-22	3	900	2015-2017	7	420
153*	122646.72	+075508.4	10	2017-04-22	3	600	2012-2017	6	300
164*	122753.57	+121735.8	90				2012-2009	6	180
171	122840.55	+091532.2	157				2015-04-14	3	300
185*	123059.71	+080440.3	90				2006-02-27	3	300
188	123139.57	+165110.1	122	2017-04-21	3	420	2015-2017	6	300
189*	123154.76	+150726.2	90	2017-05-27	3	600	2012-03-16	3	300
230	123951.91	+151752.1	90	2017-05-26	3	600	2015-03-20	4	300
232*	124057.53	+115444.0	31	2017-05-27	3	600	2012-03-15	3	300
239	124240.96	+141745.0	157	2017-05-27	3	600	2015-03-23	3	240
249	124445.99	+122105.2	72				2015-04-14	3	420
253	124717.52	-024338.6	22	2017-04-22	3	480	2015-2017	5	300
258	124835.91	-054803.1	90				2015-03-20	3	180
259	124911.56	+032319.4	90	2017-05-26	3	600	2015-03-20	3	240
266	125101.09	-062335.0	125	2017-05-27	3	600	2015-03-23	3	240
267	125145.96	+254638.3	33	2017-04-20	3	480	2015-2017	6	300
270	125222.11	-011158.9	90				2015-03-20	3	180
282	125533.67	+081425.8	90				2015-03-20	3	240
289	130848.74	-064639.1	90				2015-04-14	3	300
291*	132030.08	+430502.3	90				2009-02-19	4	300
298*	134744.99	+381816.6	90	2017-04-20	4	420	2012-2017	6	300
302*	135411.26	+051338.8	178	2017-05-26	3	600	2012-2017	11	300
303*	135445.99	+584000.7	90	2017-04-20	3	480	2009-2017	6	360
313*	142113.11	+032608.8	90	2017-04-21	3	600	2009-2017	14	300

Table A.1. Galaxies observed at the Cassini Telescope. An asterisk marks galaxies whose red spectrum was published in Gavazzi et al. (2011) or Gavazzi et al. (2013). The spectrum of HRS110 is a combination of a red spectrum taken at Loiano and a blue spectrum from the SDSS (DR7), whose red part near H α was damaged.

³ Columns are: (1): HRS name; (2) and (3): J2000 Celestial coordinates; (4): Position Angle (P.A.) of the slit with respect to N (counterclockwise); (5): Observing date (blue grism); (6): Number of exposures (blue grism); (7): Exposure time (in seconds) of the individual exposures (blue grism); (8): Observing date (red grism); (9): Number of exposures (red grism); (10): Exposure time (in seconds) of the individual exposures (red grism)

HRS	Mass M_{\odot}	$g-i$ mag	$H\alpha$ correction \AA	$H\alpha$ EW \AA	$H\alpha$ EW corr \AA	$[\text{NII}](6583)\text{EW}$ \AA	rms count	WHAN
(1)	(2)	(3)	(4)	(5)	(6)	(7)	(8)	(9)
9	10.08	1.081	1.82	1.69	3.51	3.12	0.04	wAGN
32	9.46	1.044	1.91	-1.28	0.63	0.85	0.02	RET
38	9.1	0.572	2.25	13.1	15.35	4.00	0.16	HII
45	10.25	1.248	1.82	0.23	2.05	1.70	0.05	wAGN
52	9.11	0.933	1.91	3.63	5.54	2.34	0.02	HII
58	8.94	0.661	2.44	3.89	6.33	1.99	0.10	HII
77	10.54	0.938	1.82	0.68	2.5	1.36	0.02	wAGN
84	9.39	0.851	1.91	-0.28	1.63	1.87	0.05	wAGN
124	9.52	0.732	2.25	4.96	7.21	-	0.18	HII
134	9.96	0.797	2.25	-1.12	1.13	-	0.11	HII
164	9.91	1.061	1.91	-1.48	0.43	-	0.02	PAS
171	9.69	0.75	2.25	14.92	17.17	5.07	0.07	HII
185	10.06	1.171	1.82	-2.61	-0.79	0.91	0.07	RET
249	9.01	0.688	2.25	1.86	4.11	1.63	0.11	HII
258	11.1	1.12	1.82	-0.31	1.51	1.16	0.06	wAGN
270	10.93	1.151	1.82	-	-	1.48	0.04	RET
282	9.3	1.055	1.91	-2.27	-0.36	-	0.05	PAS
289	10.31	0.281	0.49	5.322	5.81	2.26	0.07	HII
291	9.86	1.075	1.91	-1.22	0.69	0.51	0.02	RET

Table A.2. Derived spectroscopic parameters for galaxies observed at Loiano with red-channel grism. ⁴

HRS	$H\alpha$ EW \AA	$H\alpha$ correction \AA	$H\alpha$ EW _C \AA	$[\text{OIII}]/H\beta$	$[\text{NII}]/H\alpha$	BPT	WHAN
(1)	(2)	(3)	(4)	(5)	(6)	(7)	(8)
2	25.78	1.56	27.34	0.40	0.33	HII	HII
28	7.63	1.35	8.98	0.58	0.34	HII	HII
33	9.93	1.55	11.49	0.61	0.45	TR	HII
51	30.81	2.01	32.82	0.58	0.29	HII	HII
65	10.98	1.86	12.84	0.89	0.25	HII	HII
86	88.48	2.34	90.83	0.58	0.25	HII	HII
98	24.54	1.86	26.40	0.77	0.25	HII	HII
108	24.30	1.79	26.09	0.19	0.27	HII	HII
110	57.05	1.75	58.80	1.43	0.17	HII	HII
118	22.14	1.77	23.91	1.63	0.17	HII	HII
132	30.36	2.76	33.12	2.66	0.16	HII	HII
148	47.51	1.83	49.34	0.8	0.23	HII	HII
153	17.03	1.52	18.55	0.29	0.33	HII	HII
188	13.98	1.96	15.94	0.41	0.31	HII	HII
189	18.17	1.74	19.91	0.61	0.27	HII	HII
230	12.77	1.71	14.48	1.86	0.3	TR	HII
232	16.90	1.89	18.79	0.23	0.3	HII	HII
239	26.97	1.44	28.42	0.41	0.39	HII	HII
253	48.64	1.24	49.88	3.0	0.28	TR	HII
259	31.36	2.05	33.41	0.23	0.41	HII	HII
266	22.78	2.34	25.12	1.04	0.18	HII	HII
267	13.71	2.07	15.78	1.81	0.29	HII	HII
298	10.63	1.67	12.31	0.95	0.34	HII	HII
302	15.85	1.97	17.83	0.59	0.33	HII	HII
303	55.10	1.95	57.05	0.53	0.34	HII	HII
313	6.36	1.41	7.76	0.12	0.45	HII	HII

Table A.3. Derived spectroscopic parameters for galaxies observed at Loiano with red and blue channel grisms. ⁵

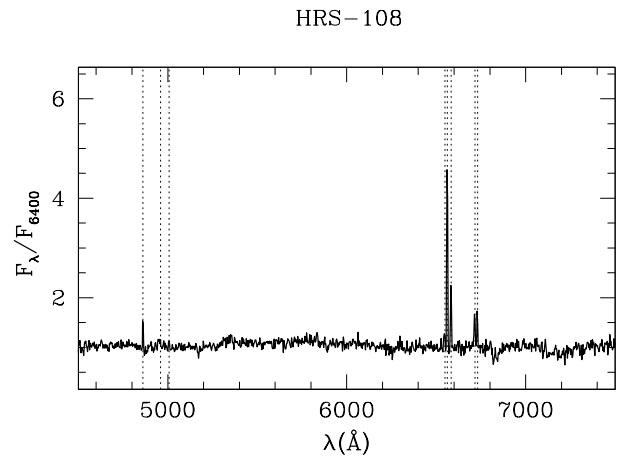
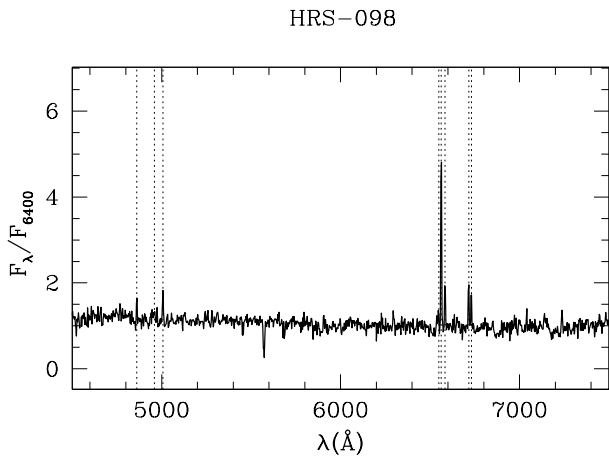
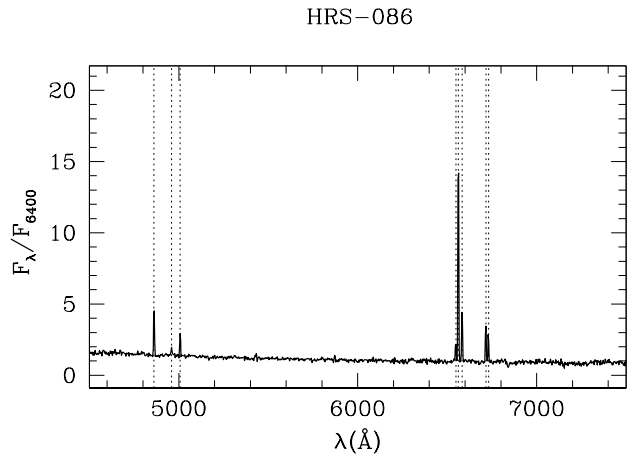
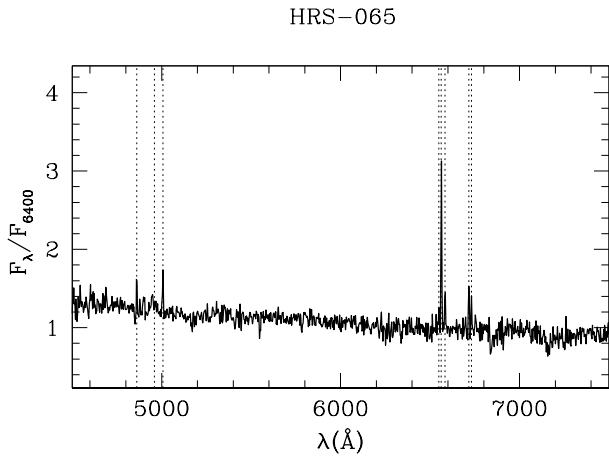
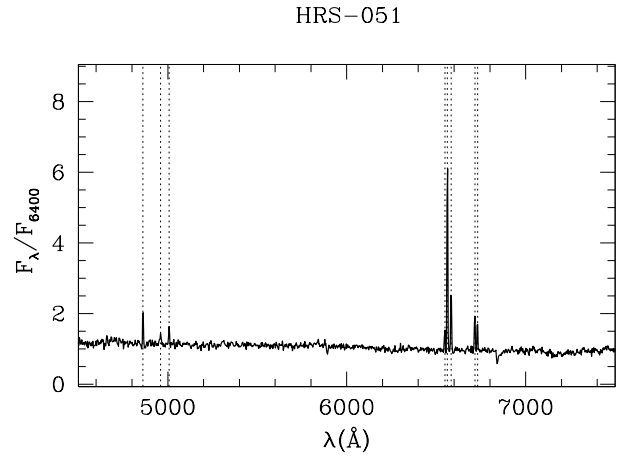
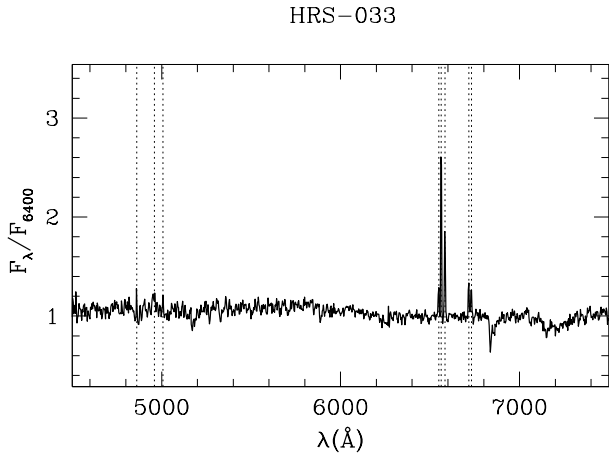
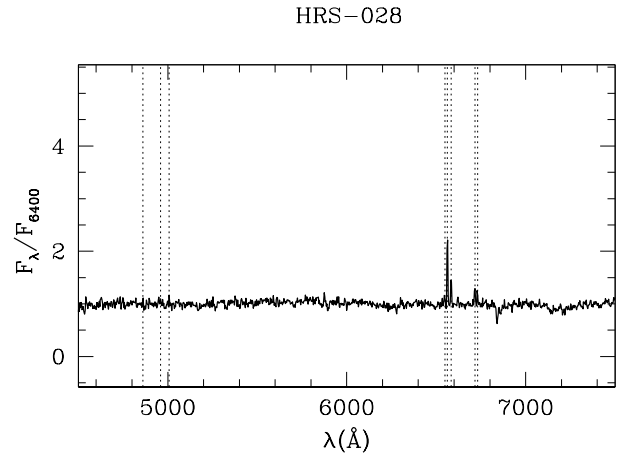
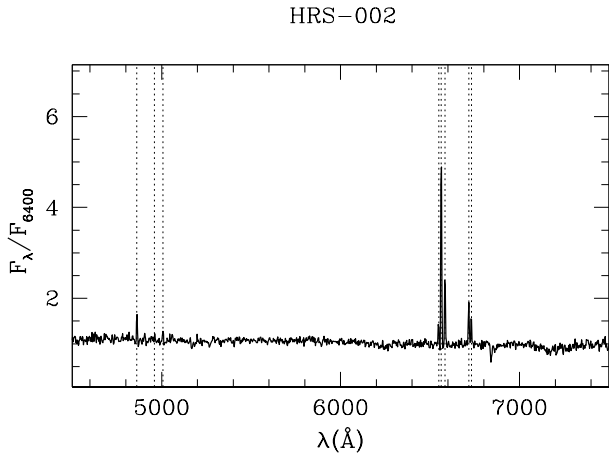
⁴ Columns are: (1): HRS name; (2): log of stellar mass M_* (M_{\odot}), from B15; (3): $g - i$ color index; (4): Absorption continuum correction to $H\alpha$ EW (see section ??); (5): Observed $H\alpha$ EW (positive EW means emission); (6): Corrected $H\alpha$ EW (positive EW means emission); (7): Observed $[\text{NII}]$ EW ($\lambda 6583 \text{ \AA}$) (positive EW means emission); (8): rms near $H\alpha$; (9): Nuclear spectral classification (from WHAN)

⁵ Columns are: (1): HRS name; (2): Absorption continuum correction to $H\alpha$ EW; (3): Observed $H\alpha$ EW (positive EW means emission); (4): Corrected $H\alpha$ EW (positive EW means emission); (5): $[\text{OIII}]/H\beta$; (6): $[\text{NII}]/H\alpha$; (7): Nuclear classification using the BPT ($[\text{NII}]/H\alpha$) diagram; (8): Nuclear classification using the WHAN diagram

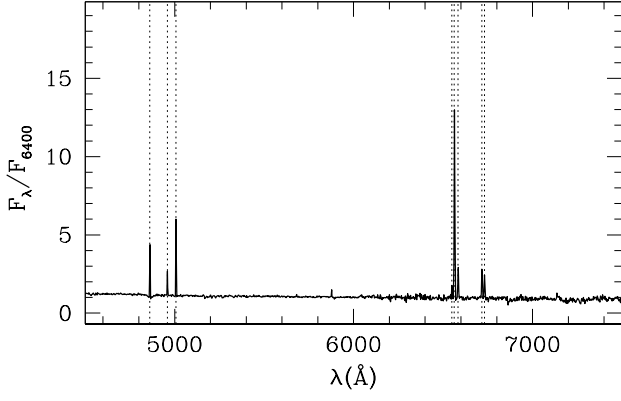
HRS	Integrated							Nuclear						
	Ref	EW $H\alpha_C$ Å	[OIII]/H β	[NII]/H α	[SII]/H α	BPT	WHAN	Ref	EW $H\alpha_C$ Å	[OIII]/H β	[NII]/H α	[SII]/H α	BPT	WHAN
(1)	(2)	(3)	(4)	(5)	(6)	(7)	(8)	(9)	(10)	(11)	(12)	(13)	(14)	(15)
1	1	18.25	0.41	0.37	0.42	HII / HII	HII	4	8.02	0.53	0.37	0.4	HII / HII	HII
2	1	30.05	0.41	0.32	0.34	HII / HII	HII	3	27.34	0.40	0.33	0.38	HII / HII	HII
3	****	****	****	****	****	**** / ****	****	5	3.93	1.58	1.16	1.19	AGN / LIN	wAGN
4	1a	10.88	3.12	0.39	0.48	AGN / SEY	sAGN	5	43.15	7.38	1.22	0.86	AGN / SEY	sAGN
5	1	6.18	-	0.89	1.14	(PAS) / (PAS)	sAGN	4	10.55	0.33	0.38	0.37	HII / HII	HII
6	****	****	****	****	****	**** / ****	****	4	6.16	0.71	0.32	0.74	HII / LIN	HII
7	2	-	-	-	-	(PAS) / (PAS)	PAS	5d	3.29	0.06	0.9	0.47	- / -	wAGN
8	****	****	****	****	****	**** / ****	****	5d	2.11	5.36	1.02	0.86	- / -	wAGN
9	****	****	****	****	****	**** / ****	****	3	3.51	-	0.89	0.83	- / -	wAGN
10	1	28.36	0.85	0.24	0.35	HII / HII	HII	4	18.86	0.42	0.29	0.41	HII / HII	HII
11	1	20.99	0.54	0.27	0.43	HII / HII	HII	4	24.13	0.28	0.32	0.33	HII / HII	HII
12	1	27.96	1.28	0.18	0.42	HII / HII	HII	4	26.63	1.14	0.17	0.39	HII / HII	HII
13	1	16.65	0.20	0.39	0.37	HII / HII	HII	4	6.94	1.63	0.68	0.31	TR / HII	sAGN
14	****	****	****	****	****	**** / ****	****	5d	1.91	-	1.26	1.68	- / -	wAGN
15	****	****	****	****	****	**** / ****	****	4	1.04	1.42	0.83	0.64	AGN / LIN	RET
16	1	12.73	0.33	0.34	0.4	HII / HII	HII	4	13.87	0.29	0.37	0.34	HII / HII	HII
17	1	30.04	0.84	0.28	0.31	HII / HII	HII	5d	5.36	0.11	0.38	0.2	- / -	HII
18	1	10.40	0.84	0.43	0.4	TR / HII	HII	4	6.98	5.91	0.68	0.73	AGN / SEY	sAGN
19	1	29.14	0.32	0.29	0.3	HII / HII	HII	4	246.83	0.18	0.30	0.19	HII / HII	HII
20	1	53.45	1.48	0.15	0.24	HII / HII	HII	5	28.47	1.0	0.33	0.4	HII / HII	HII
21	1	11.25	0.73	0.27	0.6	HII / HII	HII	4	7.67	0.68	0.33	0.7	HII / LIN	HII
22	****	****	****	****	****	**** / ****	****	5	2.26	1.32	1.18	0.94	AGN / LIN	wAGN
23	1	10.97	0.85	0.49	0.5	TR / HII	HII	4	13.61	0.41	0.52	0.39	TR / HII	sAGN
24	1	18.07	0.32	0.41	0.33	HII / HII	HII	5	17.45	0.21	0.36	0.25	HII / HII	HII
25	1	22.48	0.47	0.35	0.36	HII / HII	HII	4	69.33	0.11	0.40	0.19	HII / HII	HII
26	1	22.10	1.05	0.25	0.47	HII / HII	HII	4	19.01	1.17	0.22	0.46	HII / HII	HII
27	1	40.10	0.61	0.28	0.29	HII / HII	HII	4	24.62	0.46	0.35	0.33	HII / HII	HII
28	1	24.24	0.54	0.28	0.33	HII / HII	HII	3	8.98	0.58	0.34	0.51	HII / HII	HII
29	1	20.69	0.78	0.25	0.46	HII / HII	HII	4	9.19	0.55	0.32	0.55	HII / HII	HII
30	1	18.99	0.52	0.31	0.42	HII / HII	HII	4	7.93	0.56	0.45	0.45	HII / HII	HII
31	1	44.07	2.19	0.11	0.27	HII / HII	HII	5	293.92	4.75	0.12	0.16	TR / SEY	HII
32	1	-0.34	-	-	-	(PAS) ,(PAS)	RET	3	0.63	-	1.35	-	- / -	RET
33	1	15.41	0.32	0.39	0.44	HII / HII	HII	3	11.49	0.61	0.45	0.49	TR / HII	HII
34	1b	9.97	0.14	0.42	0.6	- / -	HII	4	3.91	0.44	0.57	0.55	TR / HII	wAGN
35	1	-0.18	-	0.16	-	(PAS) ,(PAS)	RET	5d	0.75	-	1.04	1.43	- / -	RET

Table A.4. Derived spectroscopic parameters of a sample of 35 HRS galaxies. The full catalog is available at the CDS in the electronic form. Columns marked **** were not observed, while columns marked - were not detected; positive EW means emission. A letter ‘a’ marks galaxies with integrated spectra remeasured by us using the GANDALF code; letter ‘b’ marks galaxies with H β SN \geq 3.0 instead letter ‘c’ marks galaxies with H α SN \geq 3.0 in the integrated spectrum; letter ‘d’ marks galaxies with nuclear H β SN \geq 3.0. In columns 6 and 12 the classification “(PAS)” is added to galaxies whose spectra do not contain H α , [NII], [OIII], H β , [SII](6716Å) and [SII](6731Å) in emission. In columns 7 and 14, two BPT classifications are reported: the first spectral type is from the BPT with [NII]/H α ratio, the second is from the BPT with [SII]/H α ratio.

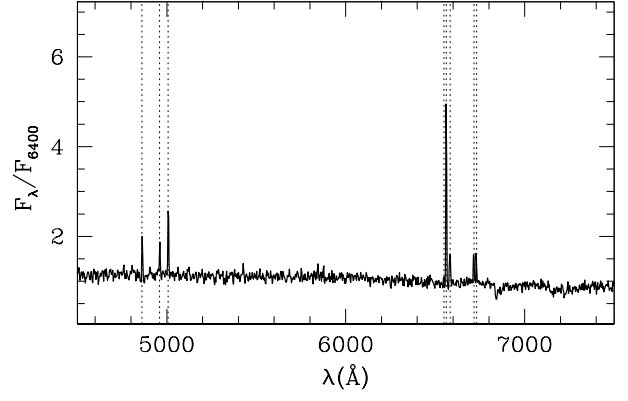
⁶ Columns 2-8 refer to integrated spectra, columns 9-15 to nuclear spectra; columns marked **** were not observed, while columns marked - were not detected; positive EW means emission. (1): HRS name; (2): Reference to the integrated spectrum: 1: B15; 2: Kennicutt et al. (1992). (3): (Integrated) H α EW corrected for continuum absorption according to GANDALF; (4): (Integrated) [OIII]/H β ; (5): (Integrated) [NII]/H α ; (6): (Integrated) [SII]/H α ; (7): (Integrated) classification using the BPT ([NII]/H α and [SII]/H α) diagrams; (8): (Integrated) classification using the WHAN diagram; (9): Reference to the nuclear spectroscopy: 3: this work or Gavazzi et al. (2013); 4: SDSS DR13 or DR12 (Albareti et al. 2016); 5: Ho et al. (1997); 6: Jones et al. (2009); 7: Veilleux et



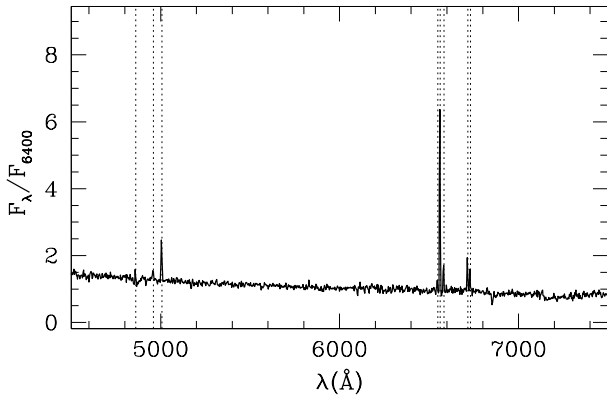
HRS-110



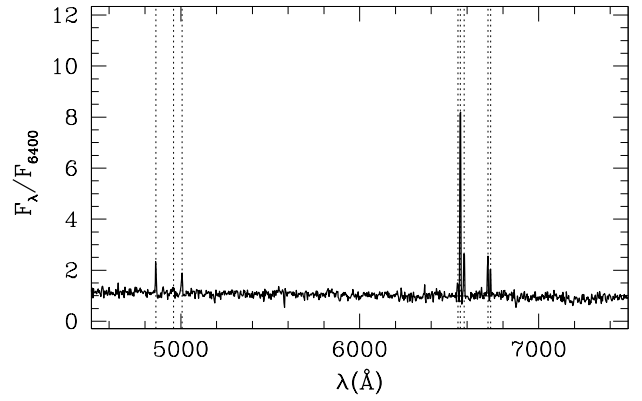
HRS-118



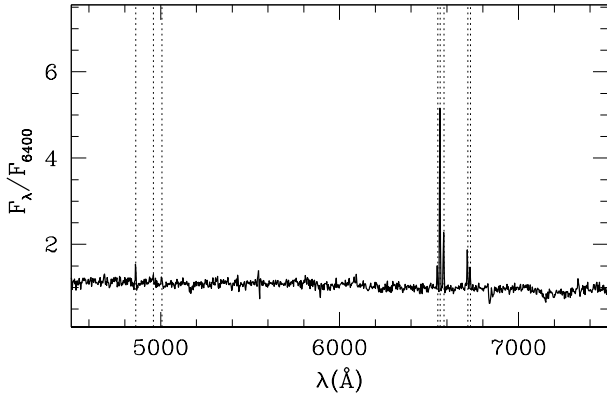
HRS-132



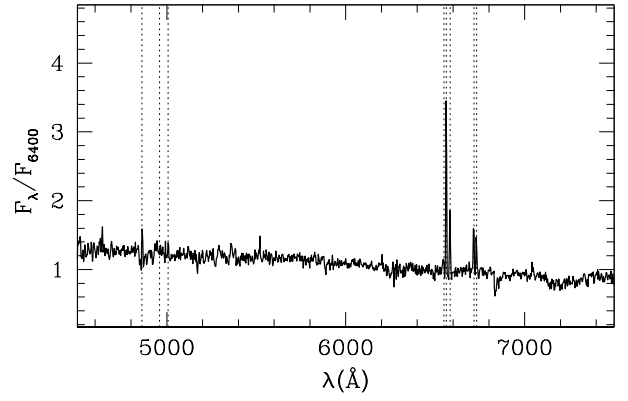
HRS-148



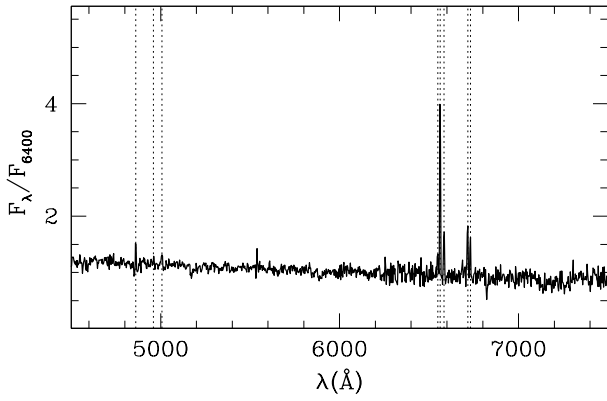
HRS-153



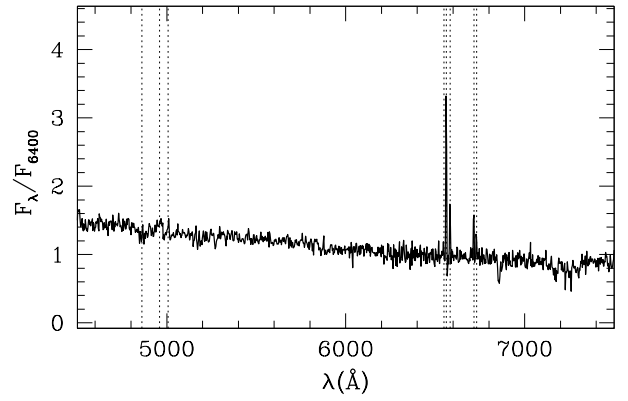
HRS-188



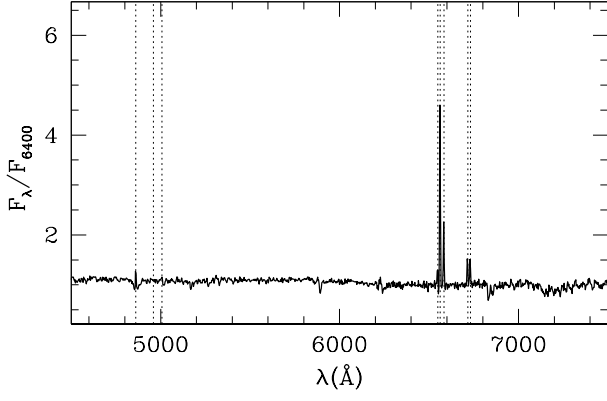
HRS-189



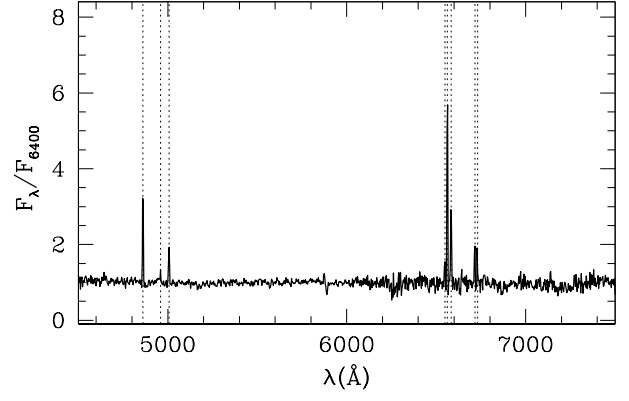
HRS-230



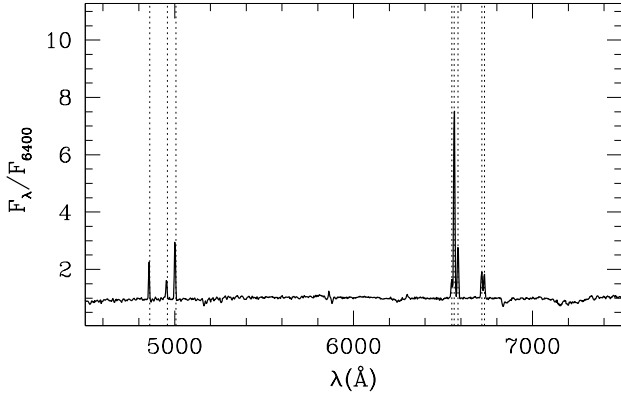
HRS-232



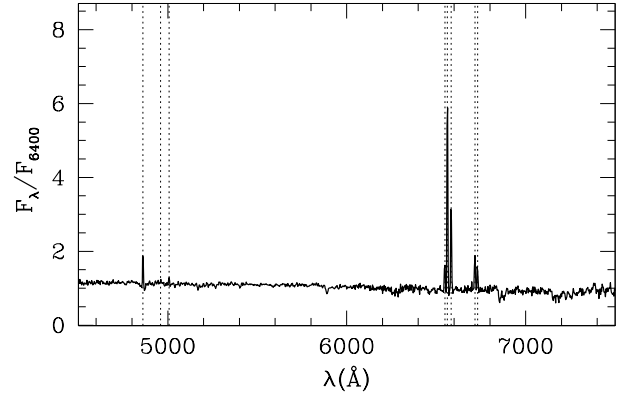
HRS-239



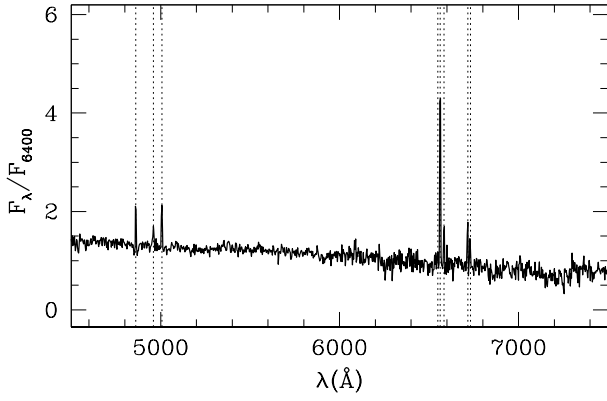
HRS-253



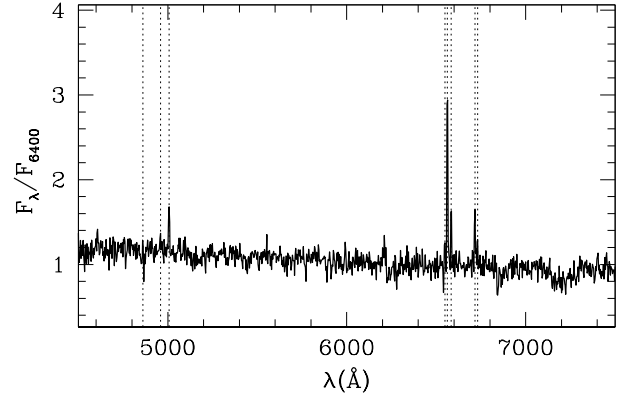
HRS-259



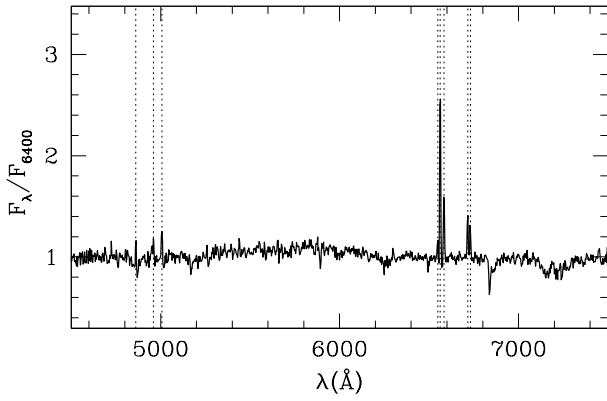
HRS-266



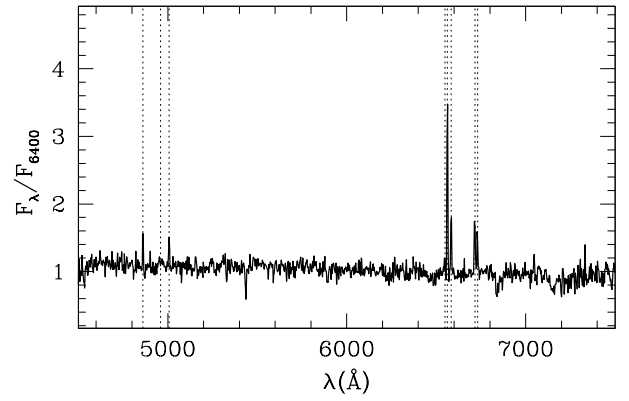
HRS-267



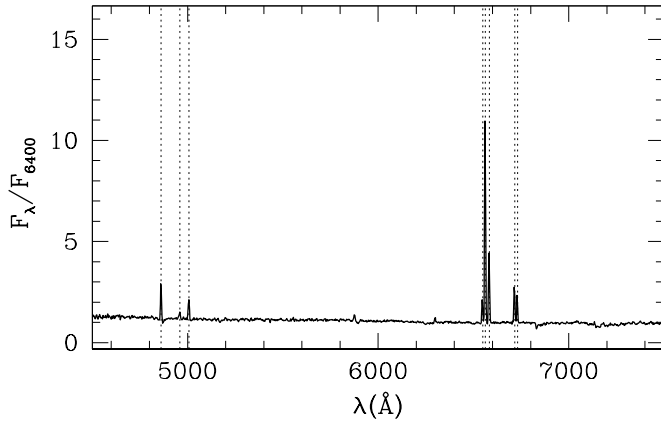
HRS-298



HRS-302



HRS-303



HRS-313

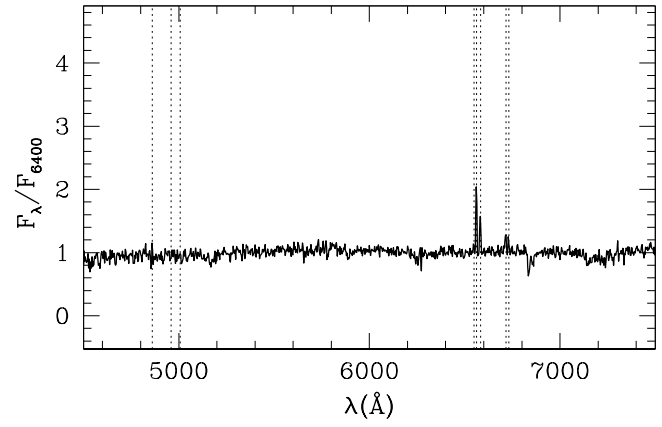
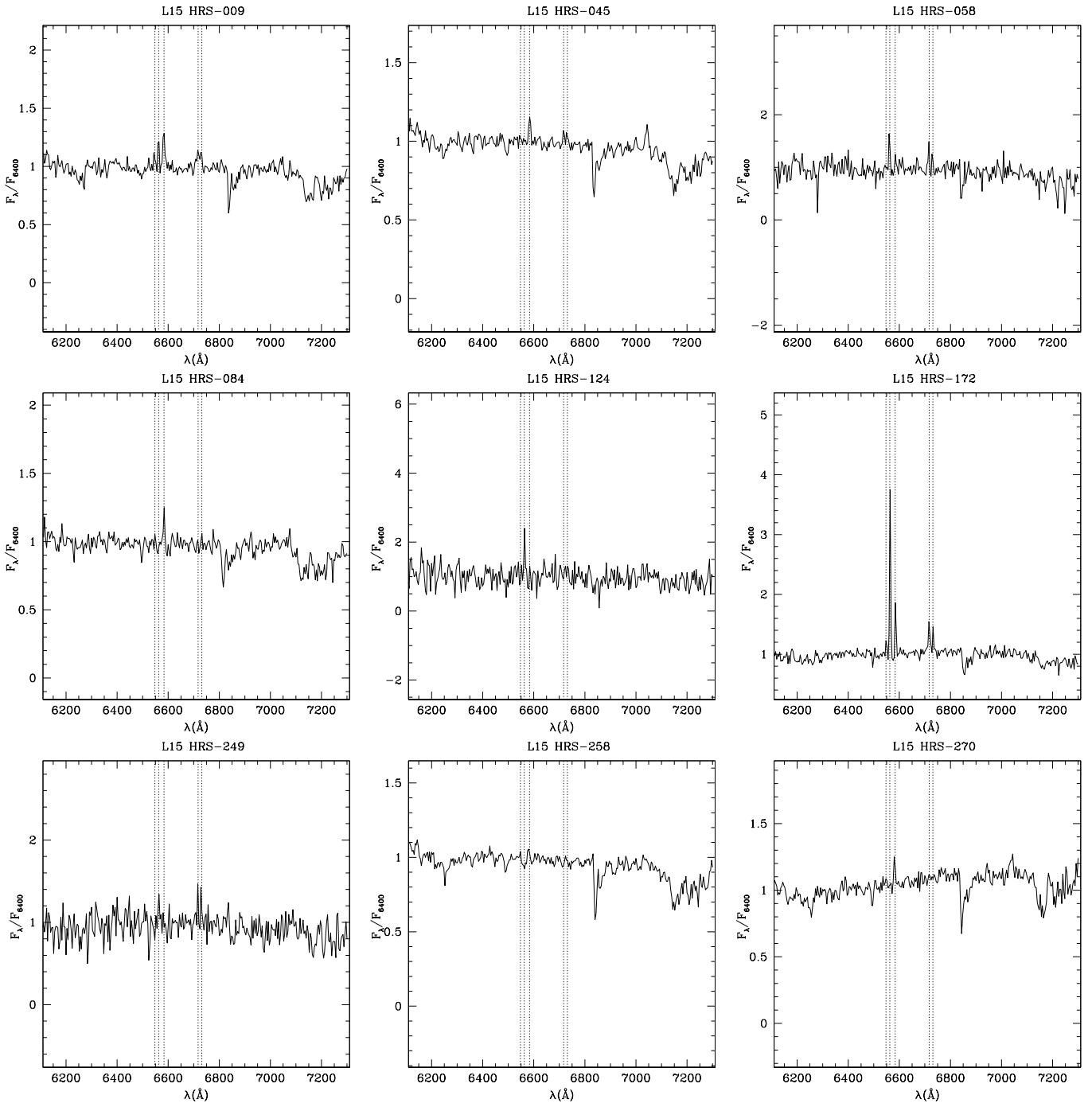


Fig. A.1: Spectra taken at Loiano with the blue and red grisms covering approximately from 4500 to 7500 Å. The spectra have been Doppler shifted to rest frame and normalized to the flux in the interval 6400-6500 Å. The vertical broken lines mark the rest-frame position of $H\beta$ λ 4861; $[OIII]$ λ 4958; $[OIII]$ λ 5007; $[NII]$ λ 6549; $H\alpha$ λ 6563; $[NII]$ λ 6584; $[SII]$ \sim λ 6717; $[SII]$ \sim λ 6731.



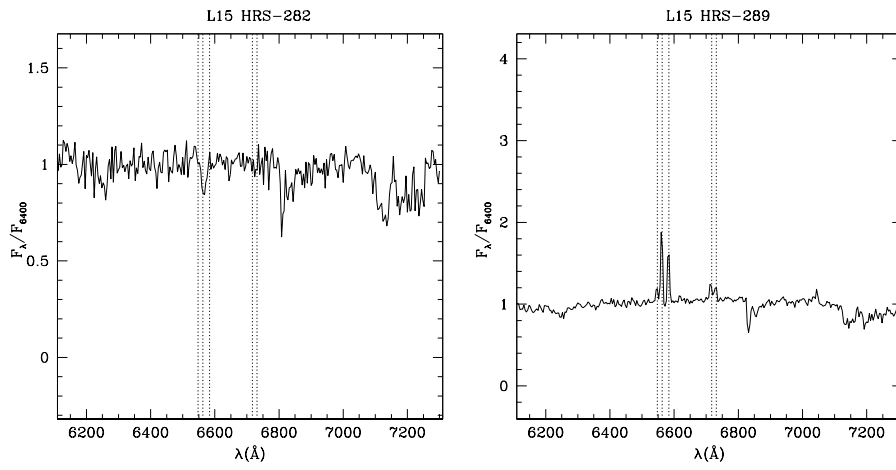
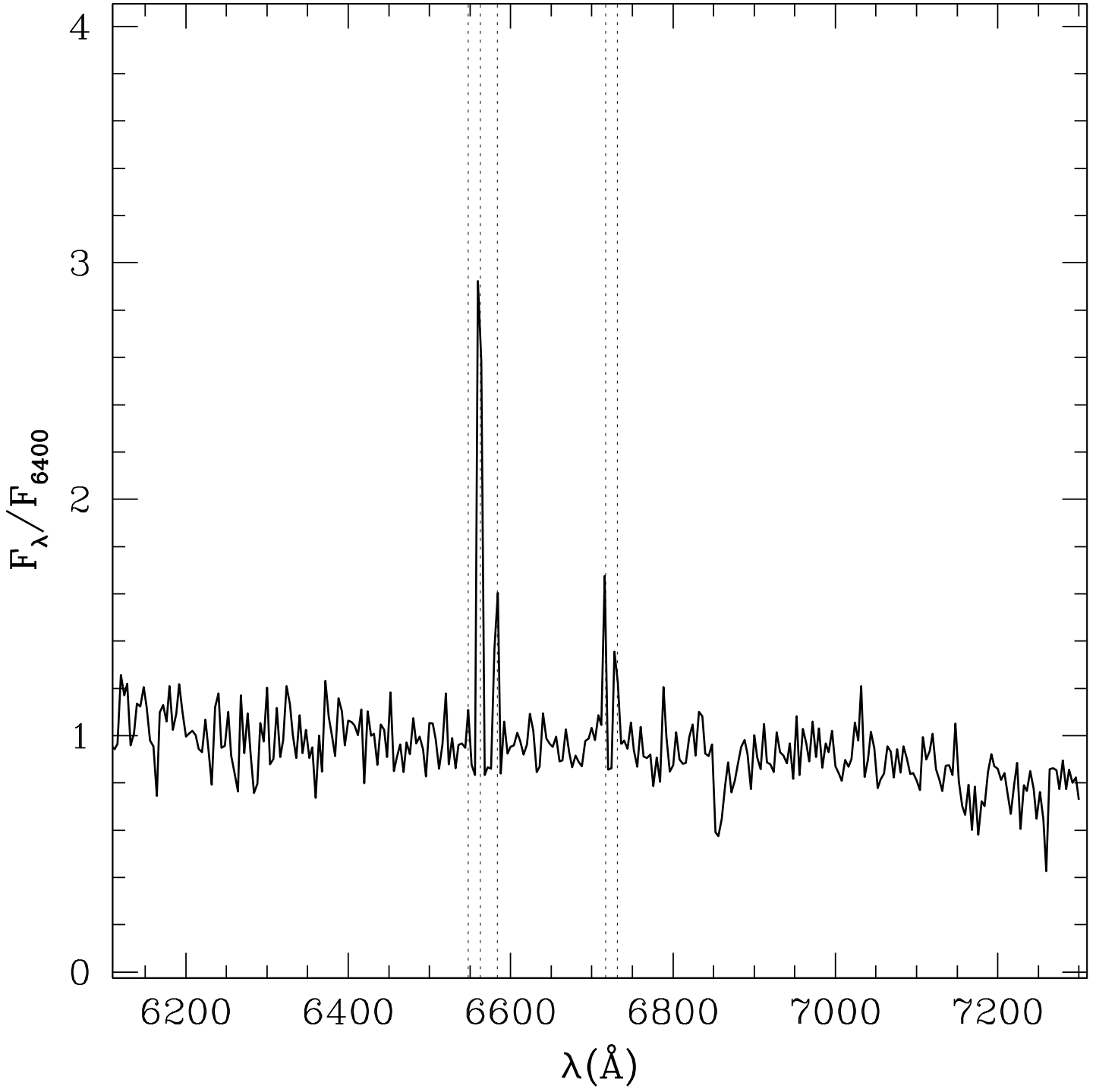


Fig. A.2: Unpublished HRS spectra taken at Loiano in 2015 with the red grism. They cover approximately from 6200 to 7200 Å. The spectra have been Doppler shifted to rest frame and normalized to the flux in the interval 6400-6500 Å. The vertical broken lines mark the rest-frame position of [NII] λ 6549; H α λ 6563; [NII] λ 6584; [SII] λ 6717; [SII] λ 6731. (Similar red-grism spectra taken prior to 2015 are already published in Gavazzi et al. 2011 and 2013)

L15 HRS-230



L15 HRS-239

